Journal of Molecular Structure 1333 (2025) 141734

Contents lists available at ScienceDirect

Journal of Molecular Structure

journal homepage: www.elsevier.com/locate/molstr

A comprehensive investigation of Schiff bases and bis-α-aminophosphonates as potent agents against Alzheimer's disease by computer-aided drug discovery techniques and in vitro examinations

Emel Ekinci [a,*], Harun Çiftçi [b,c], Şevki Adem [d], Özlem Gündoğdu Aytaç [e], Volkan Eyüpoğlu [d]

[a] Çankırı Karatekin University, Central Research Laboratory Application and Research Center, Çankırı, Türkiye
[b] Department of Medical Biochemistry, Faculty of Medicine, Kırşehir Ahi Evran University, Kırşehir, Türkiye
[c] Department of Chemistry, Institute of Science, Çankırı Karatekin University, Çankırı, Turkey
[d] Department of Chemistry, Çankırı Karatekin University, Çankırı, Türkiye
[e] Vocational School of Kaman, Ahi Evran University, Kırşehir, Türkiye

ARTICLE INFO

Keywords:
Alzheimer's disease
Cholinesterase
Enzyme inhibition
Molecular docking
Molecular dynamics
DFT

ABSTRACT

In this study, we designed and synthesized new Schiff bases (**7**–**11**) and bis-α-aminophosphonate derivatives (**13**–**16**) to examine their inhibitory properties against acetylcholinesterase (AChE) and butyrylcholinesterase (BChE) enzymes which are associated with Alzheimer's disease (AD). All newly synthesized compounds were characterized by FT-IR, ^{1}H, and ^{13}C NMR and were tested were appraised for their inhibitory potential opposite to AChE and BChE enzymes, by determining their IC_{50} and K_i values. Bis-α-aminophosphonate derivatives showed significantly strong inhibitory affinity against AChE, whereas they had weak inhibitory activities against BChE. Schiff bases exhibited low inhibitory activity against both AChE and BChE. Among bis-α-aminophosphonates, compounds **14, 15**, and **16** showed excellent inhibitory properties against AChE with an IC_{50} value of 6.48, 9.00, and 10.88 μM, respectively, with respect to positive control pyridostigmine bromide (IC_{50}= 26.2 μM). Kinetic studies showed that the inhibition mechanism of **14, 15,** and **16** against AChE is non-competitive. The physicochemical properties of compounds and their affinities towards the protein were investigated by quantum chemical calculations, molecular docking, and molecular dynamics simulation techniques. So, among the investigated compounds, compound **15** has been found as significantly higher binding affinity against AChE. This observation hints at the capacity of these compounds to potentially influence enzyme activity, indicating their potential relevance in the realm of treatment of Alzheimer's disease.

1. Introduction

Alzheimer's disease (AD) is a degenerative illness that causes cognitive impairment, emotional and behavioral changes, and physical and functional decline [1–3]. The current global Alzheimer's patient population is estimated at around 50 million, with projections showing that number rising to 150 million by the year 2050 [3–5]. Although AD has been studied for years, only four FDA-approved drugs are currently used for its symptomatic treatment. These drugs are tacrine, donepezil, rivastigmine, and galantamine [6]. Tacrine and donepezil are synthetic drugs, whereas rivastigmine and galantamine are derived from plants [6].

The pathogenesis of AD is complex and encompasses several molecular, cellular, and neurochemical alterations. An important factor in the pathogenesis of AD is the malfunction of the cholinergic system, specifically the lack of acetylcholine (ACh), a vital neurotransmitter for cognitive functioning. In AD, cholinergic neurons gradually deteriorate, leading to a significant decrease in ACh levels in key brain areas that are involved in learning and memory [7,8]. The deficiency in cholinergic function is worsened by the presence of acetylcholinesterase (AChE) activity, which reduces the amount of ACh that is available. The cognitive deterioration seen in AD is mostly caused by the disturbance in cholinergic neurotransmission. Therefore, it is crucial to target cholinergic dysfunction in therapeutic approaches to effectively treat the condition [9,10].

Current pharmacological therapies for AD are predicated on the cholinergic theory. As a result, the aim is to increase the ACh level. One way to do this is to affect cholinesterase (ChE) activity [11].

* Corresponding author.
E-mail address: emelekinci@karatekin.edu.tr (E. Ekinci).

https://doi.org/10.1016/j.molstruc.2025.141734
Received 9 August 2024; Received in revised form 22 January 2025; Accepted 10 February 2025
Available online 12 February 2025

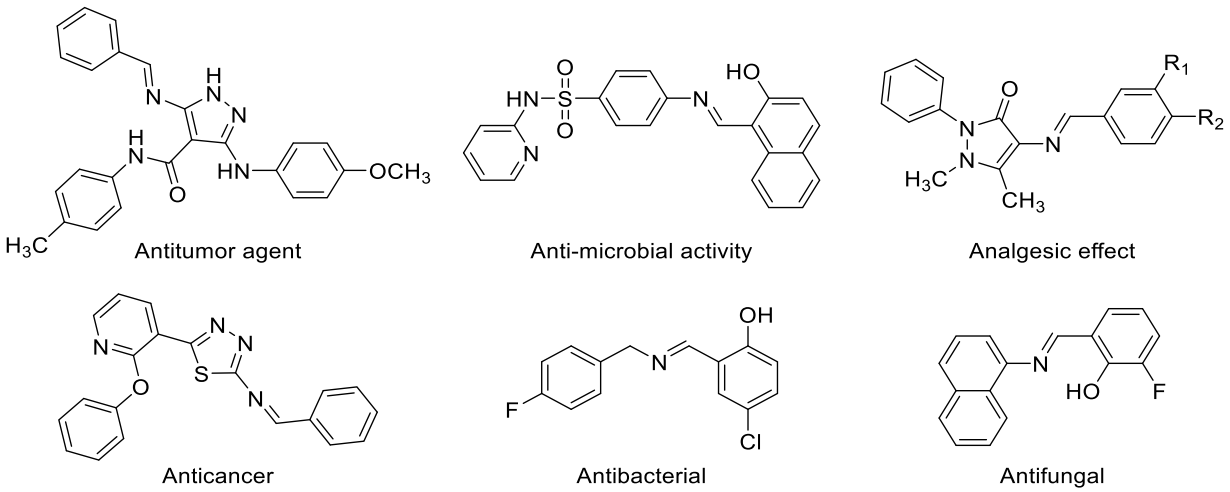

Scheme 1. Some Schiff bases with biological activity.

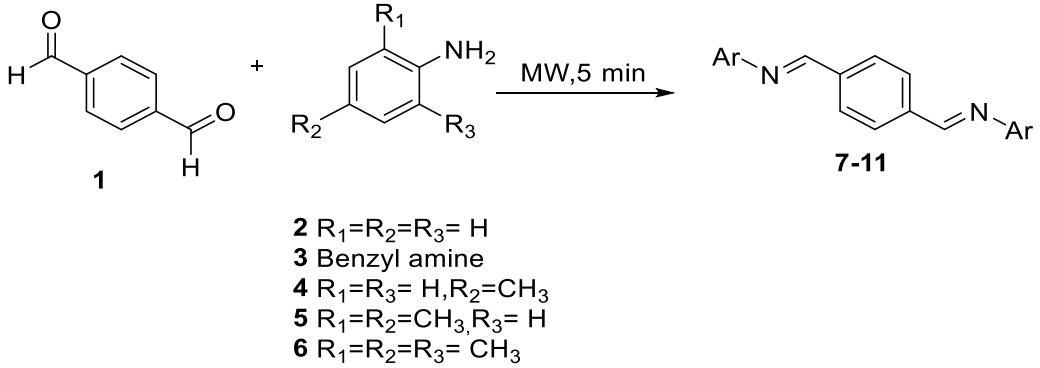

Scheme 2. General procedure for the synthesis of Schiff base compounds **7–11**.

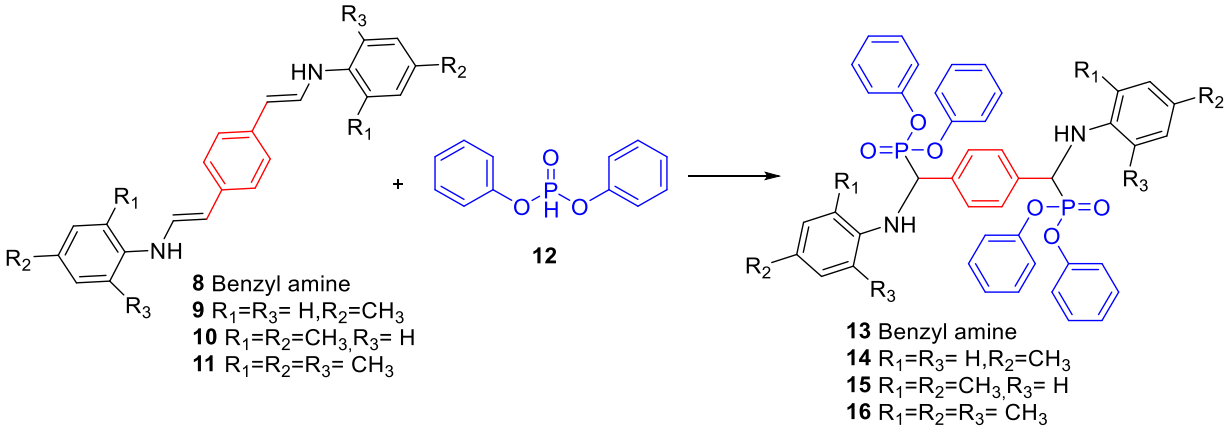

Scheme 3. General procedure for the synthesis of bis-α-aminophosphonates compounds **13–16**.

Cholinesterase inhibitors catalyze the hydrolysis of ACh with a neurotransmitter [12]. Therefore, cholinesterase inhibitors are needed to slow the onset and progression of the disease. There are two cholinesterase enzymes, acetylcholinesterase (AChE) and butyrylcholinesterase (BChE), in the human [13]. The AChE plays an important role in the degradation of ACh in the early stages of AD, while BChE compensates for the role of AChE in the late stages of AD [14,15].

Schiff bases are an important class of heterocyclic compounds containing nitrogen atoms in their structure and exhibit various biological properties. Schiff bases demonstrate anticonvulsant, antidepressant, anti-inflammatory, analgesic, antimicrobial, antimalarial, anticancer, and antioxidant activities [16,17]. Schiff bases are formed through the condensation of amines with aldehydes or ketones. These compounds were first synthesized in 1864 by the German scientist Hugo Schiff and play a significant role in the synthesis of numerous physiologically and medically active substances [18]. Additionally, Schiff bases and their derivatives are recognized as crucial intermediates in the synthesis of nitrogen-containing heterocyclic compounds. Represented by the general formula R-CH═N-Ar, Schiff bases form aldimine (azomethine) bonds when the carbonyl compound is an aldehyde and ketimine

(imine) bonds when it is a ketone [19,20]. The chemical structures of some pharmacologically active Schiff bases are shown below (Schemes 1-3).

Schiff bases exhibit diverse biological activities, including anti-inflammatory, antimicrobial, anticancer, antioxidant, antimalarial, antifungal, antiviral, analgesic, anticonvulsant, antituberculosis, and anthelmintic effects [21,22]. Some also inhibit acetylcholinesterase, making them valuable in neurodegenerative disease research [23]. Recent studies have focused on Schiff bases highlighting their enhanced biological activity and enzyme inhibition potential [24].

Organophosphorus compounds have been the focus of attention due to their natural chemical and pharmacological properties in medicinal chemistry [25]. Specifically, α-aminophosphonates are a significant class of compounds that are made of organophosphorus [26]. α-Aminophosphonates are structural analogs of amino acids with phosphorus and are of great interest because they are used for many purposes, from enzyme inhibitors to anticancer drugs [27,28]. For example, Shaik and co-workers synthesized a series of N-substituted pyrazole-derived α-aminophosphonates and evaluated their anti-cholinesterase activities. Some of these tested compounds showed significantly better AChE inhibitory activity compared to standard drugs (tacrine, rivastigmine, and galantamine) [29]. Uparkar et al. have investigated α-aminophosphonates bearing a furan ring for potential anti-Alzheimer activity. In their study, all compounds showed quite good inhibition against BChE (IC_{50} = 2.30–18.59 μM) and AChE (IC_{50} = 0.88–4.46 μM) [30]. Rao et al. synthesized and assessed a series of hybrids with quinazolinone, vanillin, and α-aminophosphonate moieties as multifunctional agents against AD. In vitro tests revealed that the majority of α-aminophosphonates possess strong and specific inhibitory effects against AChE in micromolar levels as compared to BChE [31]. Furthermore, bis-α-aminophosphonates, which are derivatives of α-aminophosphonates, also show significant biological activities and can be easily synthesized from Schiff bases and diamines [23].

In this study, we aimed to synthesize some new Schiff bases and bis-α-aminophosphonates to characterize them with various spectroscopic methods and to evaluate inhibitory properties against AChE and BChE with in vitro and *in silico* studies.

2. Materials and methods

2.1. Chemicals, reagents, and devices

All reagents used were obtained from commercial sources unless explicitly stated differently, and all solvents were subjected to distillation before their use. Melting points were determined using Gallenkamp melting point equipment. The IR spectra were obtained using the PerkinElmer Spectrum One FT-IR spectrometer. The NMR spectra were obtained using Varian 400 MHz and Bruker 400 MHz spectrometers for ^{1}H and ^{13}C nuclei. Analytical data was acquired using LECO CHNS-932 equipment for elemental analysis.

2.2. General synthesis of schiff bases

Schiff bases **7–11** were synthesized using the protocols indicated in the literature [18]. Terephthalaldehyde (**1**) (1 mmol) was added to aniline (**2**), benzylamine (**3**), p-methylaniline (**4**), 2,4-dimethylaniline (**5**), or 2,4,6-trimethylaniline (**6**) (2 mmol) and then the reaction mixture was exposed to microwave radiation at 900 W. All aromatic aniline derivatives had their reactions finished in 5 mins, according to TLC monitoring. Both the ^{1}H and ^{13}C NMR spectra pointed to the formation of a single product. The ^{1}H NMR and ^{13}C NMR spectra revealed that these compounds with a (*E*)-configuration generated a single product.

2.3. Physical properties and spectral data of synthesized compounds

1,1′-(1,4-phenylene)bis(N-benzylmethanimine) (7): Yield: 96 %, yellow solid, m.p. 108–109 °C. **^{1}H NMR** (400 MHz, $CDCl_3$) δ 8.45 (s, 2H), 7.87 (s, 4H), 7.41 – 7.38 (m, 6H), 7.35 – 7.27 (m, 2H), 4.88 (s, 4H). **^{13}C NMR** (100 MHz, $CDCl_3$) δ 161.38, 139.09, 138.18, 128.57, 128.52, 128.06, 127.11, 65.19. **FT-IR (cm-1):** 1640(C=N), 1494 (C=C aromatic), 1453, 1437, 1368(C—N), 1297. **Chemical Formula**: $C_{22}H_{20}N_2$. **Exact Mass:** 312.42. **Elemental Analysis:** 84.58; H, 6.45; N, 8.97 **Found:** C, 84.11; H, 6.70; N, 9.18.

1,1′-(1,4-phenylene)bis(N-phenylmethanimine) (8): Yield:94 %, yellow solid, m.p. 158–159 °C. **^{1}H NMR** (400 MHz, $CDCl_3$) δ 8.55 (s, 2H), 8.05 (s, 4H), 7.49 – 7.42 (m, 5H), 7.33 – 7.25 (m, 5H). **^{13}C NMR** (100 MHz, $CDCl_3$) δ 159.46, 151.77, 138.67, 129.24, 129.16, 126.35, 120.96. **FT-IR (cm-1):** 1614 (C=N), 1581, 1477(C=C aromatic), 1187, 1162, 829. **Chemical Formula:** $C_{20}H_{16}N_2$. **Exact Mass:** 284,13. **Elemental Analysis:** 84.48; H, 5.67; N, 9.85 **Found:** C, 84.46; H, 5.64; N, 9.88.

1,1′-(1,4-phenylene)bis(N-p-tolylmethanimine) (9): Yield: 95 %, yellow solid, m.p. 189–190 °C. **^{1}H NMR** (400 MHz, $CDCl_3$) δ 8.55 (s, 2H), 8.02 (s, 4H), 7.33 – 7.13 (m, 8H), 2.42 (s, 6H). **^{13}C NMR** (100 MHz, $CDCl_3$) δ 158.62, 149.15, 138.66, 136.28, 129.85, 129.03, 120.92, 21.06. **FT-IR (cm-1):** 2872, 1639 (C=N), 1494 (C=C aromatic), 1357, 1296, 1188, 1107, 966. **Chemical Formula:** $C_{22}H_{20}N_2$. **Exact Mass:** 312,42. **Elemental Analysis:** 84.58; H, 6.45; N, 8.97 **Found:** C, 84.55; H, 6.47; N, 8.98.

1,1′-(1,4-phenylene)bis(N-(2,4-dimethylphenyl)methanimine) (10): Yield: 94 %, yellow solid, m.p. 134–135 °C. **^{1}H NMR** (400 MHz, $CDCl_3$) δ 8.46 (s, 1H), 8.04 (s, 2H), 7.12 – 7.04 (m, 2H), 6.93 (d, J = 7.9 Hz, 1H), 2.41 (s, 3H), 2.38 (s, 3H). **^{13}C NMR** (101 MHz, $CDCl_3$) δ 157.81, 148.22, 138.82, 135.83, 132.36, 131.20, 128.94, 127.24, 117.21, 20.97, 17.81. **FT-IR (cm-1):** 2914, 1622 (C=N), 1485 (C=C aromatic), 1354, 1300, 1193, 973, 856, 805. **Chemical Formula:** $C_{24}H_{24}N_2$. **Exact Mass:** 340.47. **Elemental Analysis:** C, 84.67; H, 7.11; N, 8.23. **Found:** C, 84.23; H, 7.42; N, 8.18.

1,1′-(1,4-phenylene)bis(N-mesitylmethanimine) (11): Yield: 96 %, yellow solid, m.p. 193–194 °C. **^{1}H NMR** (400 MHz, $CDCl_3$) δ 8.31 (s, 2H), 8.06 (s, 4H), 6.94 (s, 4H), 2.33 (s, 6H), 2.17 (s, 12H). **^{13}C NMR** (100 MHz, $CDCl_3$) δ 162.02, 148.54, 138.59, 133.27, 128.80, 128.77, 126.98, 20.78, 18.23. **FT-IR (cm-1):** 2849, 1631(C=N), 1475(C=C aromatic), 1353, 1298, 1193, 1140,1101, 1033, 1011, 976, 846. **Chemical Formula:** $C_{26}H_{28}N_2$. **Exact Mass:** 368.52. **Elemental Analysis:** 84.74; H, 7.66; N, 7.60. **Found:** C, 84.67; H, 7.65; N, 7.56.

2.4. Synthesis of bis-α-aminophosphonate

After the imine compounds **8–11** were dissolved in ethanol, the diphenyl phosphonate **12** was added slowly at room temperature. Everything was combined until a white precipitate was produced. The filtrate was then let to air dry at ambient temperature [32].

2.5. Physical properties and spectral data of synthesized compounds

Tetraphenyl(1,4-phenylenebis((benzylamino)methylene))bis (phosphonate) (13): Yield: 91 %, white solid, m.p. 156–157 °C. **^{1}H NMR** (400 MHz, $CDCl_3$) δ 7.61 (s, 4H), 7.40 – 7.25 (m, 14H), 7.23 – 7.04 (m, 12H), 6.92 (dd, J = 5.7, 2.7 Hz, 4H), 4.46 (dd, J = 19.2, 2.4 Hz, 2H), 3.94 (d, J = 13.2 Hz, 2H), 3.68 (dd, J = 13.2, 2.7 Hz, 2H). **^{13}C NMR** (100 MHz, $CDCl_3$) δ 150.65, 150.60, 150.45, 150.40, 138.84, 135.13, 129.66, 129.59, 129.38, 128.52, 128.49, 127.37, 125.14, 125.03, 120.62, 120.60, 120.40, 120.38, 60.08, 58.51, 51.44. **FT-IR (cm-1):** 3310 (C—NH),1589 (C=C aromatic), 1486 (C=C aromatic), 1455, 1251, 1209, 1187, 1157, 929. **Chemical Formula:** $C_{46}H_{42}N_2O_6P_2$. **Exact Mass:** 780.80. **Elemental Analysis:** C, 70.76; H, 5.42; N, 3.59. **Found:** C, 70.78; H, 5.39; N, 3.62.

Tetraphenyl(1,4-phenylenebis((p-tolylamino)methylene))bis (phosphonate) (14): Yield: 92 %, white solid, m.p. 202–203 °C. **^{1}H NMR** (400 MHz, $CDCl_3$) δ 7.58 (d, J = 3.5 Hz, 4H), 7.31 – 7.20 (m, 4H), 7.19 – 7.02 (m, 12H), 6.96 (dd, J = 7.7, 5.9 Hz, 4H), 6.78 (dd, J = 11.2,

Table 1
Global reactivity parameters (in eV) for **7–11** and **13–16** compounds.

Compound	ΔE	I	A	χ	μ	η	σ	ω
7	4.546	−0.493	−7.808	−4.151	4.151	7.315	0.137	1.177
8	3.630	−1.027	−7.218	−4.123	4.123	6.191	0.162	1.373
9	3.525	−0.972	−6.972	−3.972	3.972	6.001	0.167	1.315
10	3.459	−0.976	−6.871	−3.923	3.923	5.895	0.170	1.306
11	3.481	−0.890	−6.827	−3.858	3.858	5.937	0.168	1.254
13	5.417	0.229	−7.351	−3.561	3.561	7.581	0.132	0.836
14	4.549	0.154	−6.699	−3.273	3.273	6.852	0.146	0.782
15	4.429	0.146	−6.566	−3.210	3.210	6.712	0.149	0.767
16	4.767	0.265	−6.746	−3.241	3.241	7.012	0.143	0.749

*Softness, σ, is given in $(eV)^{-1}$.

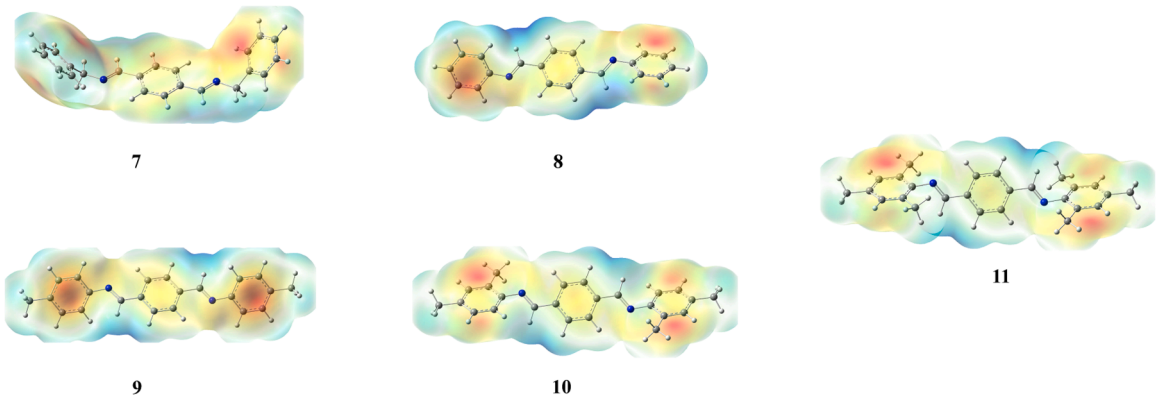

Fig. 1. The MEP maps of compounds **7–11** at the B3LYP/cc-pVDZ level.

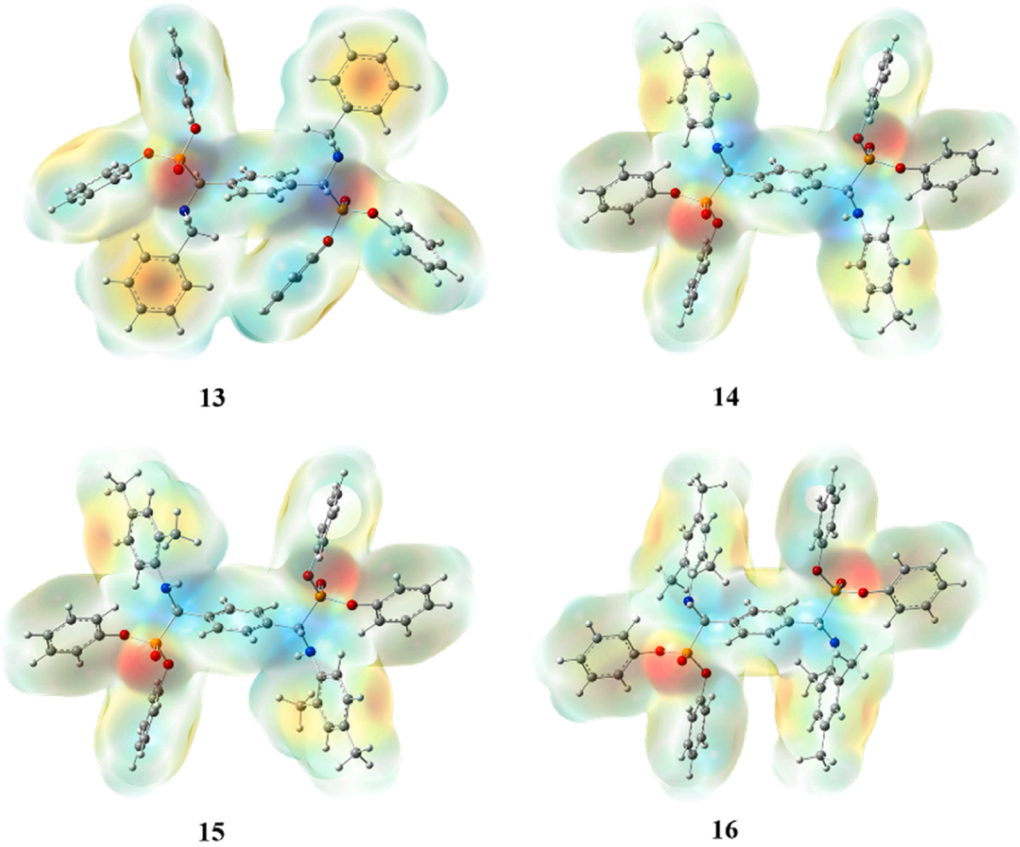

Fig. 2. The MEP maps of compounds **13–16** at the B3LYP/cc-pVDZ level.

Table 2
The results of the inhibition studies of all compounds on AChE and BChE enzymes.

Compound	AChE IC_{50} (μM)	Inhibition Type	BChE IC_{50} (μM)
7	115.52	-	693.15
8	99.02	-	315.07
9	92.42	-	433.22
10	113.63	-	407.73
11	138.63	-	346.57
13	43.32	-	49.51
14	9.00	Non-competative	231.05
15	6.48	Non-competative	173.29
16	10.88	Non-competative	223.59
Pyridostigmine bromide	**26.2**		**141.50**

8.2 Hz, 4H), 6.57 (dd, J = 8.4, 2.3 Hz, 4H), 5.17 (d, J = 26.2 Hz, 2H), 2.26 (s, 6H). **^{13}C NMR** (100 MHz, $CDCl_3$) δ 150.37, 150.12, 150.07, 150.02, 143.56, 143.33, 135.40, 129.84, 129.75, 129.71, 129.65, 128.71, 128.13, 127.98, 125.38, 125.22, 125.16, 120.75, 120.68, 120.35, 120.28, 114.13, 55.95 (d, 1C), 20.42. **FT-IR (cm-1):** 3307 (NH), 1588(C=C aromatic), 1521(C=C aromatic), 1486, 1253, 1208, 1184, 1161, 931, 904. **Chemical Formula:** $C_{46}H_{42}N_2O_6P_2$. **Exact Mass:** 780.80. **Elemental Analysis:** C, 70.76; H, 5.42; N, 3.59. **Found:** C, 70.75; H, 5.46; N, 3.56.

Tetraphenyl(1,4-phenylenebis(((2,4-dimethylphenyl)amino) methylene))bis(phosphonate) (15): Yield: 92 %, white solid, m.p. 152–153 °C. **^{1}H NMR** (400 MHz, $CDCl_3$) δ 7.58 (s, 4H), 7.24 (ddd, J = 20.1, 13.2, 9.3 Hz, 4H), 7.20 – 7.11 (m, 6H), 7.11 – 7.02 (m, 4H), 6.82 (dt, J = 12.1, 5.9 Hz, 6H), 5.31 – 5.09 (m, 2H), 2.23 (s, 6H), 2.19 (s, 6H). **^{13}C NMR** (101 MHz, $CDCl_3$) δ 150.49, 150.46, 150.10, 150.05, 141.49, 141.41, 135.39, 131.27, 129.73, 129.69, 128.56, 127.81, 127.32, 127.29, 125.37, 125.23, 123.41, 120.58, 120.30, 111.56, 56.03 (d, 1C), 20.36, 17.43. **FT-IR (cm-1):** 3312 (NH), 1590(C=C aromatic), 1514 (C=C aromatic), 1487(C=C aromatic), 1268, 1207, 1182, 1159, 932. **Chemical Formula:** $C_{48}H_{46}N_2O_6P_2$. **Exact Mass:** 808.85. **Elemental Analysis:** C, 71.28; H, 5.73; N, 3.46. **Found:** C, 71.24; H, 5.77; N, 3.48.

Tetraphenyl (1,4-phenylenebis((mesitylamino)methylene))bis (phosphonate) (16): Yield: 89 %, white solid, m.p. 159–160 °C. **^{1}H NMR** (400 MHz, $CDCl_3$) δ 7.49 (d, J = 5.6 Hz, 4H), 7.29 (dd, J = 9.0, 6.5 Hz, 4H), 7.23 – 7.10 (m, 10H), 7.06 (t, J = 7.3 Hz, 2H), 6.78 (t, J = 9.4 Hz, 8H), 4.80 (dd, J = 22.2, 5.4 Hz, 2H), 2.24 (s, 6H), 2.17 (s, 6H), 2.16 (s, 6H). **^{13}C NMR** (100 MHz, $CDCl_3$) δ 150.44, 150.36, 150.27, 150.16, 140.96, 140.90, 136.40, 131.70, 131.67, 129.75, 129.68, 129.57, 129.38, 129.34, 128.88, 128.82, 125.16, 125.06, 120.63, 120.38, 59.12 (d, 1C), 20.52, 18.69, 18.67. **FT-IR (cm-1):** 3310 (NH), 1590(C=C aromatic), 1485(C=C aromatic), 1265, 1205, 1183, 1158, 922. **Chemical Formula:** $C_{50}H_{50}N_2O_6P_2$. **Exact Mass:** 836.91. **Elemental Analysis:** C, 71.76; H, 6.02; N, 3.35. **Found:** C, 71.79; H, 6.07; N, 3.39.

2.6. Global reactivity descriptors

Geometry optimization of the compounds and harmonic vibration frequency calculations were carried out using the density functional theory (DFT) method, B3LYP functional [33,34] and cc-pVDZ basis set [35]. Global reactivity parameters are important quantum chemical parameters that enable us to understand the chemical reactivity and kinetic stability of compounds. These parameters are used to predict molecular interactions in biochemistry and molecular biology [36,37]. They also provide information about the electronic properties of compounds and their interactions with biological receptors. The Gaussian 16

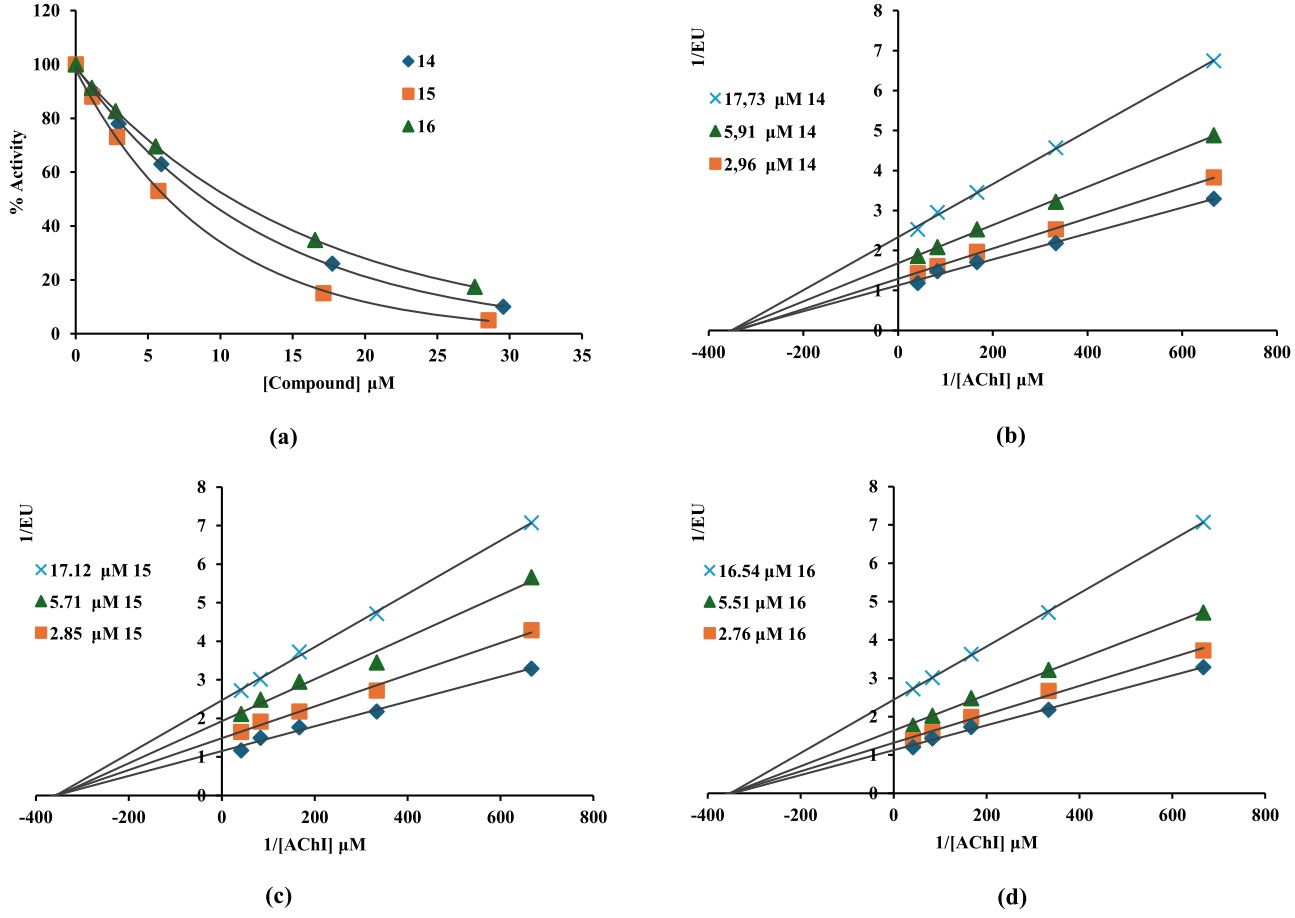

Fig. 3. (a) IC_{50} graph., Lineweaver–Burke plot of the inhibition kinetics of AChE for **14** (b), **15** (c), and **16** (d).

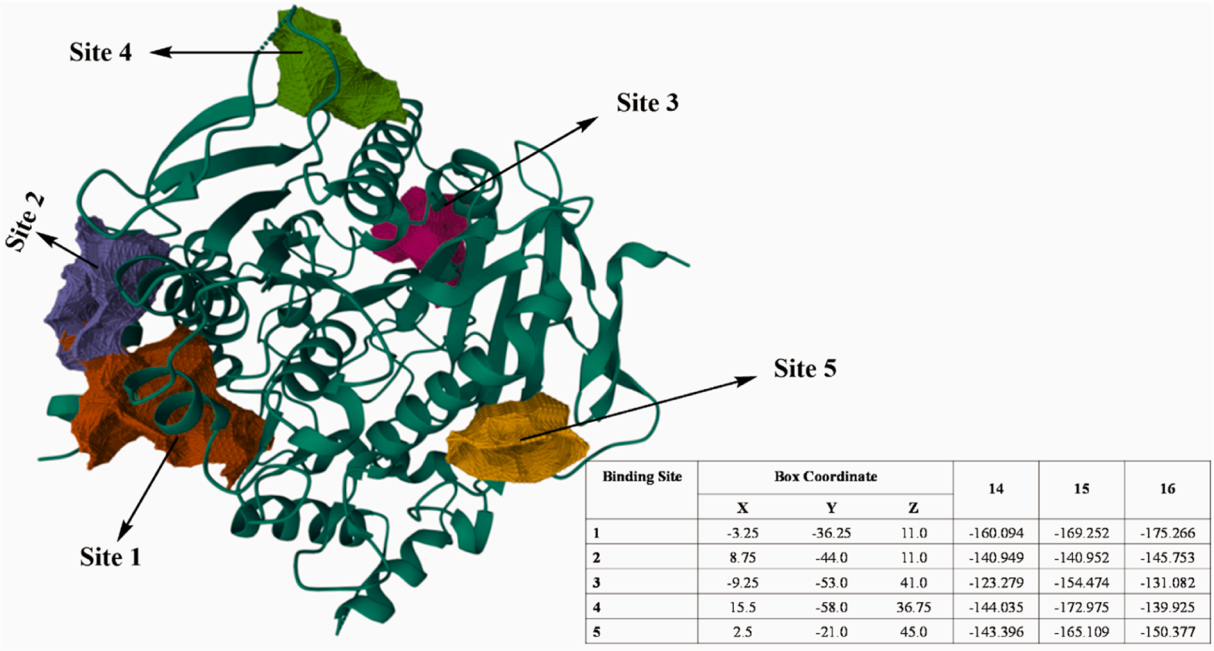

Binding Site	Box Coordinate			14	15	16
	X	Y	Z			
1	-3.25	-36.25	11.0	-160.094	-169.252	-175.266
2	8.75	-44.0	11.0	-140.949	-140.952	-145.753
3	-9.25	-53.0	41.0	-123.279	-154.474	-131.082
4	15.5	-58.0	36.75	-144.035	-172.975	-139.925
5	2.5	-21.0	45.0	-143.396	-165.109	-150.377

Fig. 4. Docking results of **14, 15**, and **16** with AChE at five different binding sites.

Table 3
Docking scores of compounds **14, 15,** and **16**.

Ligand	MolDock Score	H Bond
14	−182.87	−0.78
15	−202.41	0
16	−191.74	1.28

program was used to do all quantum chemical computations [38].

2.7. Cholinesterase inhibitory activities

To measure the activity of cholinesterase enzymes, Ellman's method was adapted to fit the needs of our laboratory [39]. Firstly, stock solutions were prepared by dissolving with DMSO at 3mg/mL and diluting fifteen times with pure water to be used in enzyme inhibition studies. Five different inhibitor concentrations were used to test the activities of the enzymes. The reaction mix for the AChE/BChE consists of 50μL of

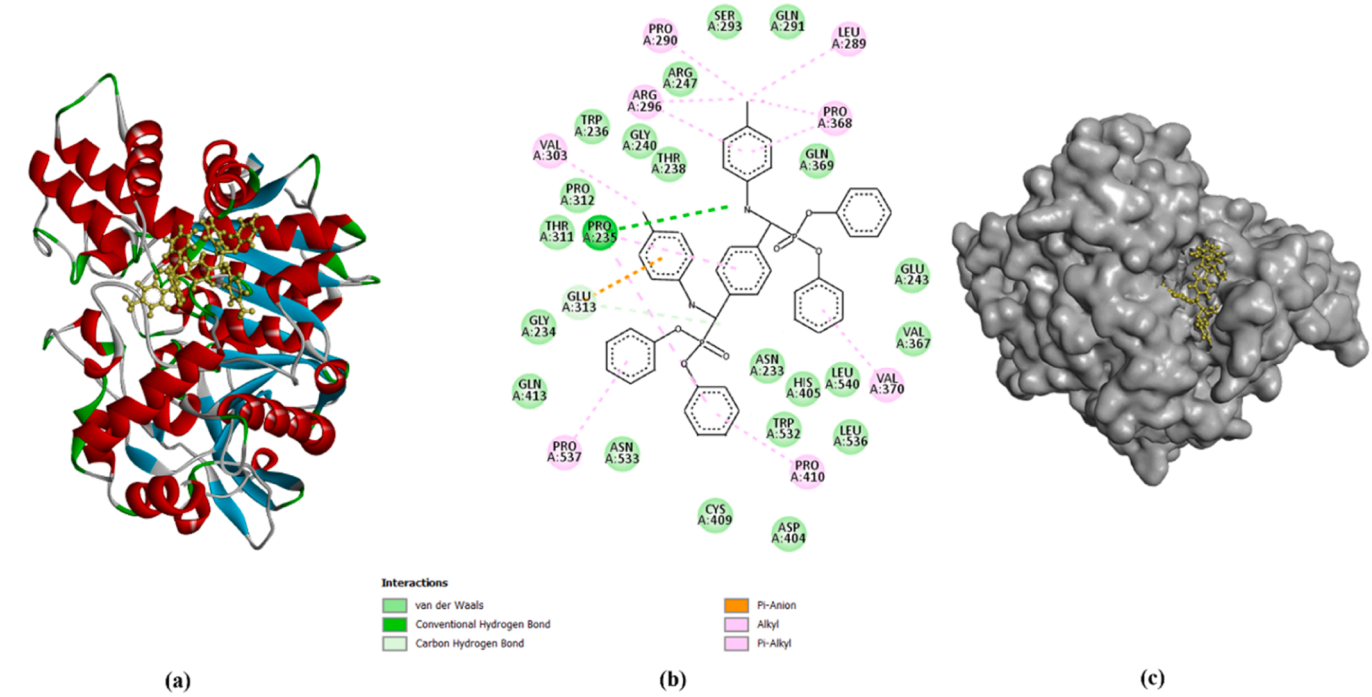

Fig. 5. Binding mode of AChE with compound **14**. (a) 3D and (b) 2D scheme of complex, and (c) Surface of the enzyme (gray) in interaction with compound **14** (yellow) at the binding site.

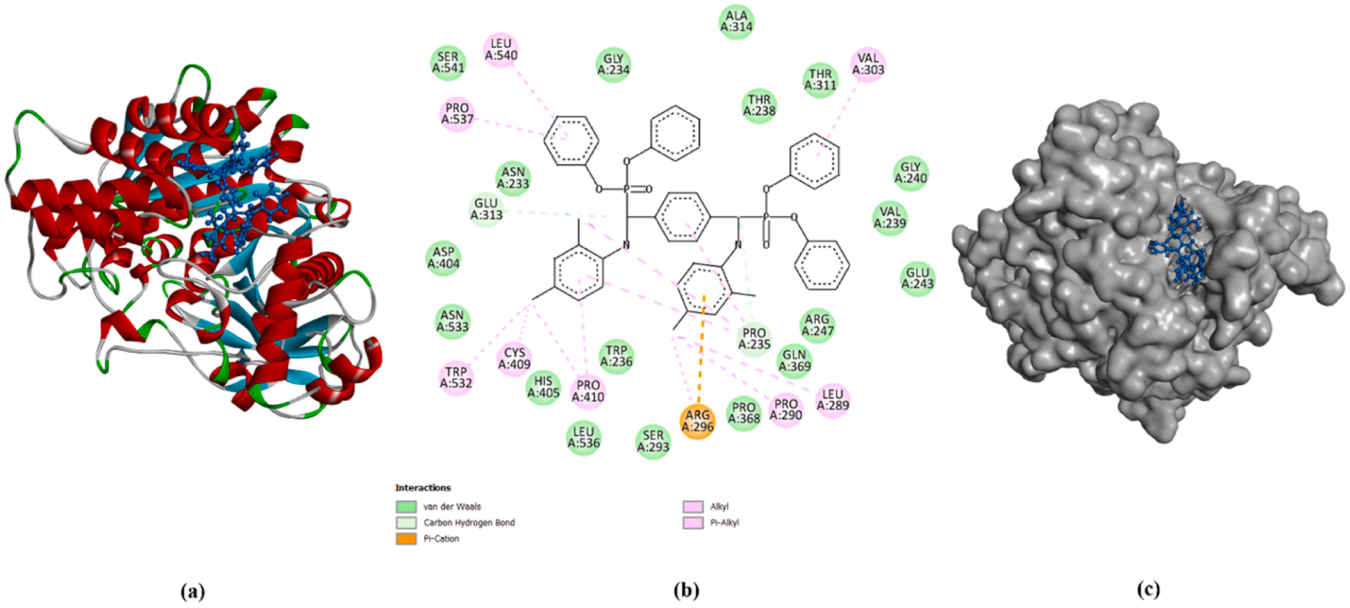

Fig. 6. Binding mode of AChE with **15**. (a) 3D and (b) 2D scheme of complex, and (c) Surface of the enzyme (gray) in interaction with compound **15** (blue) at the binding site.

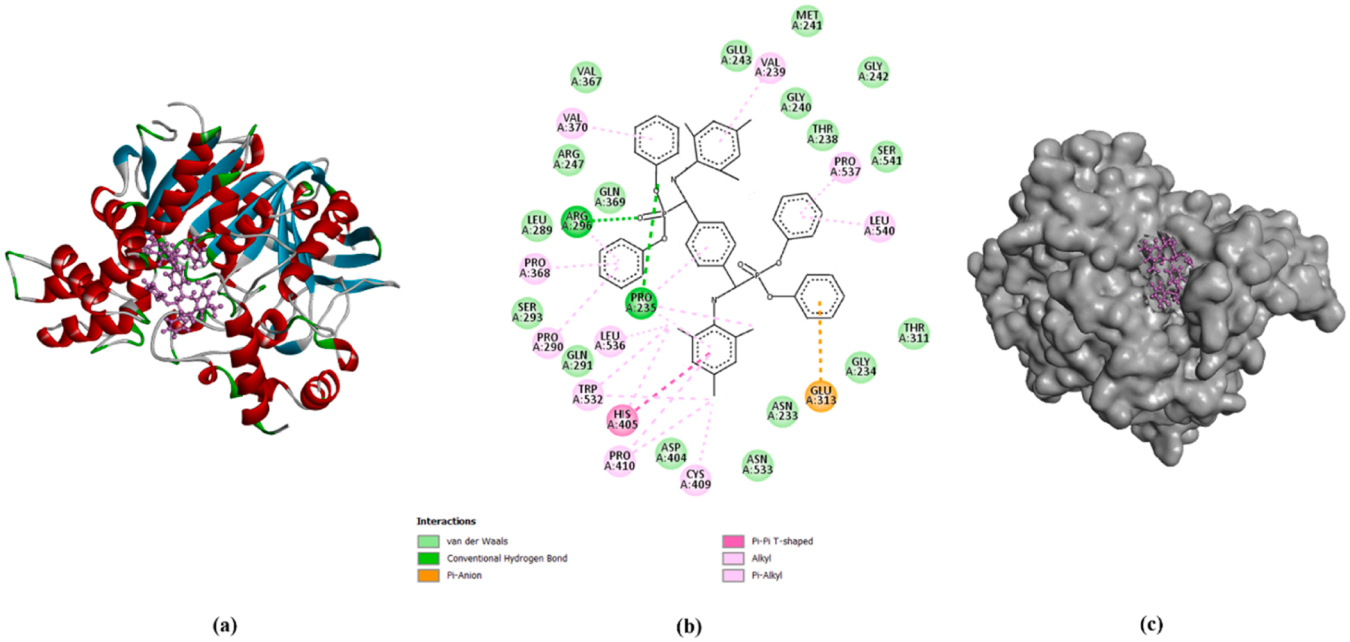

Fig. 7. Binding mode of AChE with **16**. (a) 3D and (b) 2D scheme of complex, and (c) Surface of the protein (gray) in interaction with compound **16** (pink) at the binding site.

distilled water, 50μL of 0.1 M Tris–HCl buffer (pH:8.0), 15μL of 0.015 M acetylcholine iodate/butyrylcholine iodide, 30μL of 0.06 M 5 5′-dithiobis(2-nitrobenzoic acid) (DTNB), and 10μL enzyme. Before adding the substrate to each well of plates, the absorbance of the blank solution was measured. Then, the reaction was started by adding the substrate. Enzyme activities were evaluated kinetically at 408 nm in a microplate reader. The IC_{50} values of the compounds were determined by drawing inhibition concentration graphs against activity %.

2.8. Enzyme kinetics

To determine the AChE inhibition type, kinetic studies were performed by different concentrations of acetylthiocholine iodide in the presence of three different concentrations of bis-α-aminophosphonate derivatives. The inhibition kinds of the synthesized compounds on enzymatic activity were determined using the Lineweaver-Burk plots (1/V) (inverse of velocities) versus 1/[S] μM^{-1}(inverse of substrate concentration). The K_i named as inhibitor constant was calculated via the formula slope $= K_m/V_{max}\ (1 + I/K_i)$ obtained from the aforementioned graphs.

2.9. Molecular docking

Molecular docking is an effective theoretical tool for investigating ligand-protein interactions, which are significant in many biological processes [40]. In order to understand the atomic level interaction

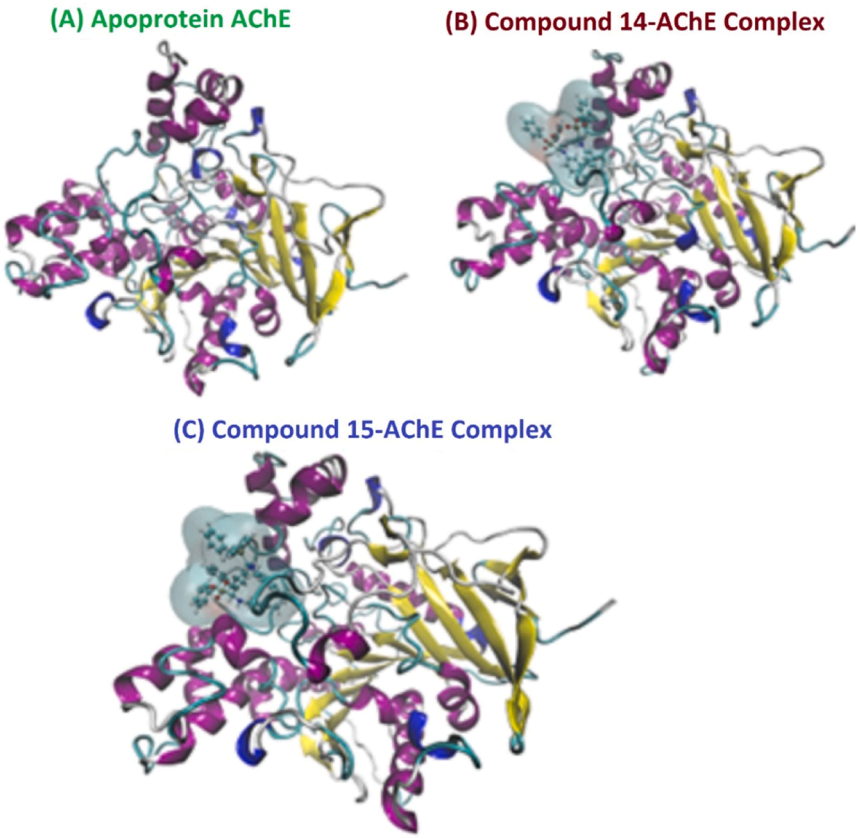

Fig. 8. Graphical representation of enzyme-ligand complexes: (A) Apoprotein AChE, (B) compound **14**-AChE, and (C) compound **15**-AChE where the protein is shown in cartoon representation and the ligand is shown in CPK representation with compound **14** parent surface.

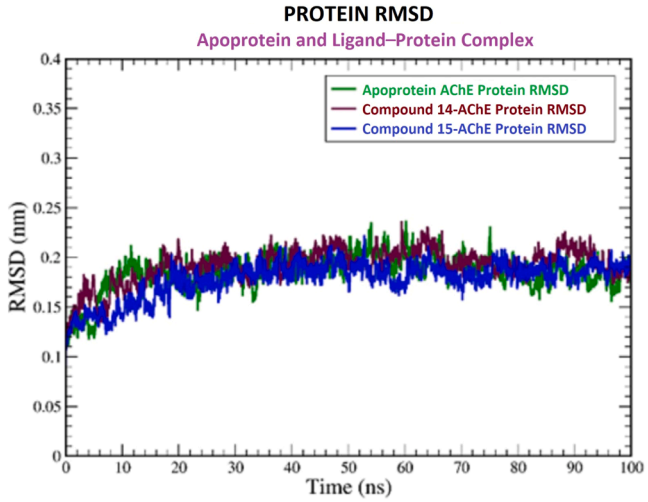

Fig. 9. Graphical representation of the plots showing Protein RMSD (nm) versus time (100 ns) for Apoprotein AChE, compound **14**-AChE, and compound **15**-AChE.

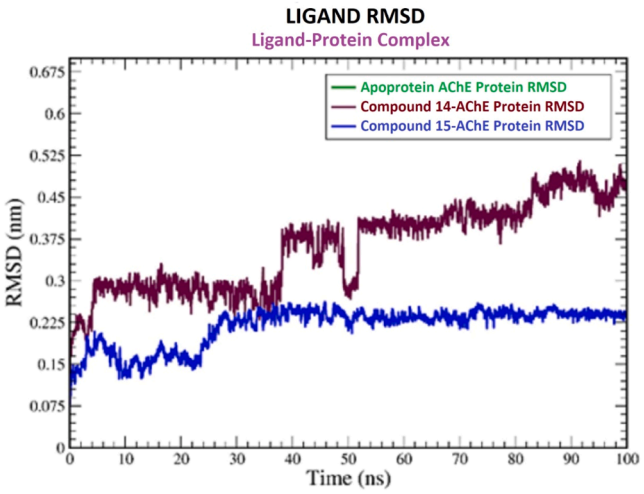

Fig. 10. Graphical representation of the plots showing Ligand RMSD (nm) versus time (100 ns) for compound **14**-AChE, and compound **15**-AChE.

between compounds and the target enzymes, AChE and BChE, molecular docking analysis was performed. Research on docking was conducted with the help of Molegro Virtual Docker 6.0 [41]. The crystal structures of AChE (4EY7), and BChE (4BDS) were received from the Protein Data Bank [42,43]. Docking procedures such as preparation of protein and ligand, removal of water molecules, and selection of the active site of the enzyme are performed automatically by the Molegro Virtual Docker program 6.0 [41]. The software BIOVIA Discovery Studio was used to visualize the many sorts of interactions and 2D binding postures that occurred between the enzymes and the compounds that were synthesized. The CavityPlus program was used to visualize potential AChE enzyme binding sites [44].

2.10. Molecular dynamic simulation

In order to simulate molecular dynamics (MD), GROMACS 2022.2 was used. These procedures were employed.

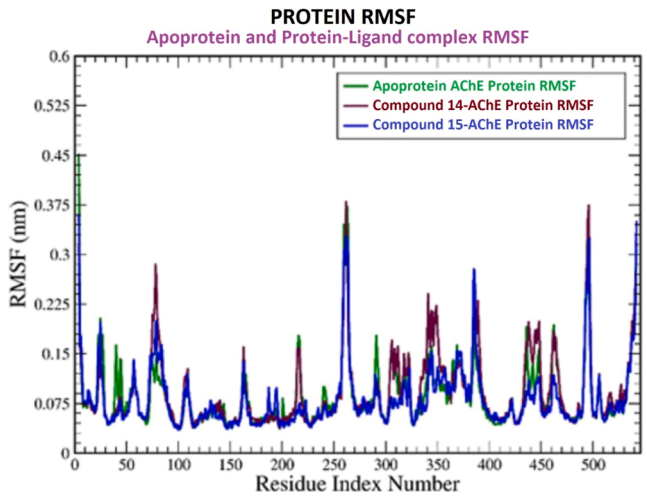

Fig. 11. Graphical representation of the plots showing the protein RMSF (nm) versus residue index number of protein for Apoprotein AChE, compound **14**-AChE, and compound **15**-AChE.

2.10.1. *Preparation of enzyme*

The apoprotein and ligand-protein complex 3D models were saved to .pdb format by use of Pymol. In order to assess the complexes' dynamic behavior, the GROMACS package program (version 2022.2) was used for molecular dynamic (MD) simulation [45,46]. Protein topology was generated using the CHARMM27 force field via pdb2gmx [47], and the SwissParam server was used to construct the ligand topology [48].

2.10.2. *Setting up system for simulation*

The system was then modified by inserting the complexes after the force field had been applied. They were solvated with the TIP3P water model [49] in a cubic box greater than 1 nm from the edge of the protein with periodic boundary conditions. After injecting Na^+ ions to neutralize the system, the steepest descent technique was used to minimize energy for 50,000 steps. To bring the system to equilibrium, 100 ps of NVT simulation at 300 K and 100 ps of NPT simulation followed. The constant-temperature, constant-pressure (NPT) ensemble used the leapfrog algorithm to link each component, such as proteins, ligands, water molecules, and ions, independently [50]. In order to maintain a steady state for the system, with a temperature of 300 K and a pressure of 1 bar, the Berendsen temperature coupling constant was set to 1 and the pressure coupling constant to 2, respectively [51]. Isothermal and isobaric condition ensembles were run in a 100 ns MD simulation at 300 K. The pressure coupling with time-constant was set at 1 ps to maintain pressure constant at 1 bar, and the LINCS algorithm [52] was used to constrain the bond lengths. The Van der Waals and Coulomb interactions were truncated at 1.2 nm, and the PME algorithm [53] inbuilt in GROMACS was used to minimize the error from truncation.

The trajectory files are visualized through VMD (Visual Molecular Dynamics) 1.9.2 [54]. and analyzed by indigenously developed tool HeroMDAnalysis [55,56] and Xmgrace 5.1.25 [57].

3. Result and discussion

3.1. *Global reactivity descriptors*

Global reactivity parameters (GRPs) can be defined by the highest occupied molecular orbital (HOMO) and lowest unoccupied molecular orbital (LUMO) energies. HOMO and LUMO play important roles in describing many properties (ionization potential, I, electron affinity, A, electronegativity, χ, chemical potential, μ, chemical hardness, η, chemical softness, σ, and electrophilicity, ω) of molecules in quantum chemistry [58,59]. GRPs for **13–16** and **7–11** were computed at the B3LYP/cc-pVDZ level by using equations in Supplementary Data, and the results are displayed in Table 1. In Schiff bases, the **10** possesses the smallest energy gap, thus it is softer and more reactive with a softness value of 0.170 eV among all the derivatives. The order of computed softness values is **10** > **11** > **9** > **8** > **7**. On the other hand, among bis-α-aminophosphonate derivatives, the **15** has the smallest energy gap, thus it is softer and more reactive with a softness value of 0.149 eV among all the derivatives. The order of computed softness values is **15** > **14** > **16** > **11**. While the computed chemical hardness values for Schiff bases are between 5.895–7.315 eV, for bis-α-aminophosphonates they are between 6.712–7.581 eV. The computed value of chemical hardness

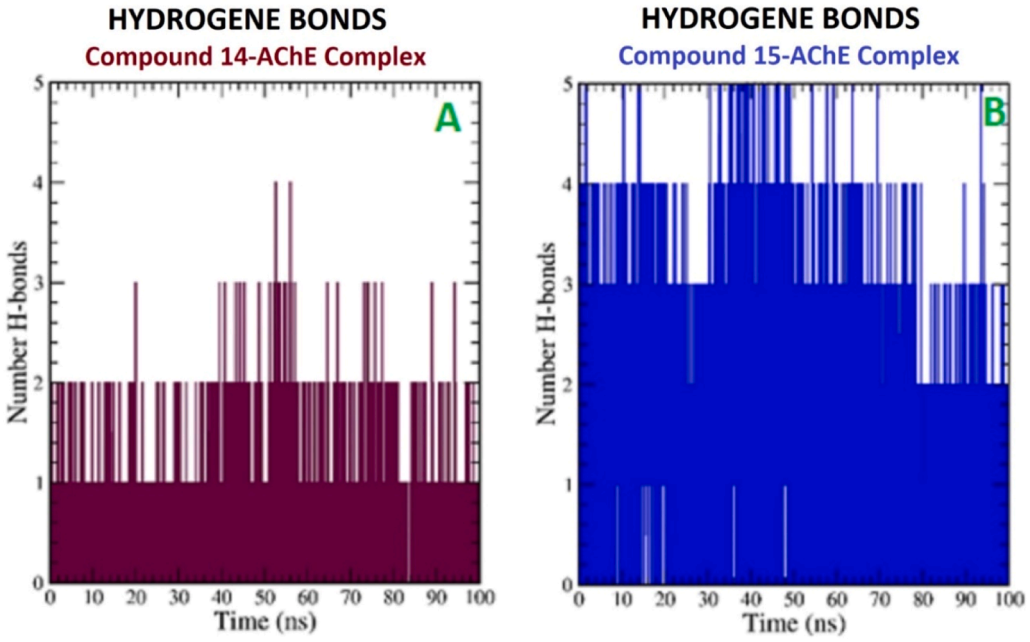

Fig. 12. Pictorial representation of the number of H-bond contacts formed by ligands, (A) compound **14**, and (B) compound **15** in complex with AChE protein (PDB ID: 4EY7).

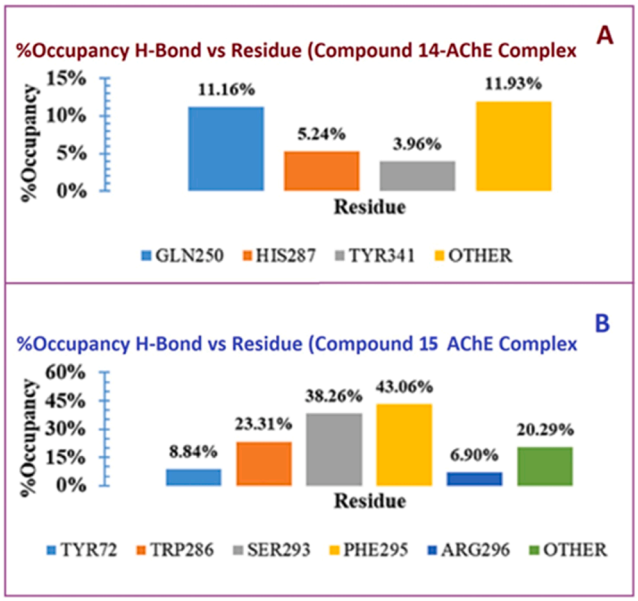

Fig. 13. Histogram representation of % occupancies of the H-bond protein-ligand contacts of (A) compound **14**, and (B) compound **15** in complex with AChE protein (PDB ID: 4EY7).

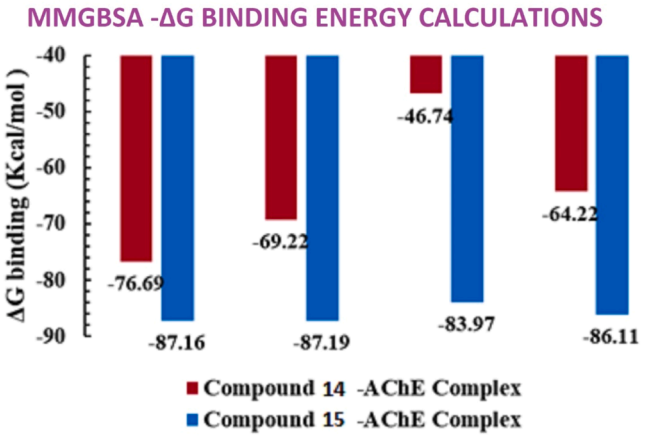

Fig. 14. MMGBSA ΔG binding energy calculations for compounds **14**, and **15** in complex with AChE protein (PDB ID: 4EY7).

Table 4
MMGBSA ΔG binding energy calculations (in kcal/mol) for compounds **14**, and **15** in complex with AChE protein (PDB ID: 4EY7).

	0 ns	50 ns	100 ns	Average
Compound 14-AChE Complex	−76.69	−69.22	−46.74	−64.22
Compound 15-AChE Complex	−87.16	−87.19	−83.97	−86.11

for **7–11** is higher (7.315 eV) than their softness (0.170 eV), which demonstrates the less reactivity and more stability of the **7**–**11**. The computed value of chemical hardness for **13–16** is higher than their softness, which demonstrates the less reactivity and more stability of the **13–16**. Additionally, the I values of all molecules are higher than their A values, indicating that the compounds' tendency to donate electrons is higher than their tendency to gain electrons. The propensity of electrons to depart from the equilibrium system is indicated by the molecule's negative electronegativity (χ) or chemical potential (μ). A more reactive and less stable molecule is one with a high chemical potential. When compared to the other compounds in the series, the chemical potential of Schiff bases **7** and **8** was determined to be greater. The electrophilicity index (ω) measures a molecule's ability to accept electrons. The fact that the I values of all compounds are lower than the electrophilicity index indicates that the molecules are electrophilic.

3.2. *Molecular electrostatic potential (MEP) maps*

Potential energy maps or molecular electrostatic potential surfaces are another name for molecular electrostatic potential (MEP) maps, which display the distribution of charges in molecules. The electron density surface is a map with colors. On these maps, the red areas represent areas with a high electron density, while the blue areas represent areas with a low electron density [60,61]. Looking at the MEP maps of **7–11**, the most electron-dense regions are on the benzene rings, while the electron-poor regions are on the hydrogen in the imine group (-N═CH-) (Fig. 1). In **13–16**, the most electron-dense regions are on the phosphonate groups, while the electron-poor regions are on the hydrogens in the amine group (-N–CH-) (Fig. 2).

3.3. *Cholinesterase inhibitory activities*

In this study, the in vitro enzyme inhibitory activities of the synthesized **7–11** and **13–16** were evaluated against AChE and BChE. The results with IC_{50} values for **7–11** and **13–16** against AChE and BChE are shown in Table 2. Positive control for AChE and BChE was performed with pyridostigmine bromide. The IC_{50} values of the synthesized compounds **7–11** against AChE range from 92.42 to 138.63 μM, while these values for **13–16** vary from 6.48 to 43.32 μM. Among the Schiff bases derivatives, the **9** showed better inhibition (IC_{50}= 92.42 μM) against AChE than the others (Table 2). On the other hand, **15** among bis-α-aminophosphonates showed the strongest inhibition with an IC_{50} value of 6.48 μM against AChE (Table 2). The order of inhibitory activities is as follows: **9** > **8** > **10** > **7** > **11** for the Schiff bases and **15** > **14** > **16** > **13** for the bis-α-aminophosphonate derivatives. When we look at Schiff bases **7** and **8**, it is seen that the benzyl group attached to the nitrogen, i.e. the chain extension in the structure, reduces the activity of the molecule against AChE. In addition, it is seen that **9**, which has a methyl group in its structure, is a stronger inhibitor against AChE than **7** and **8**. However, increasing the number of methyl groups in the structure (compounds **10, 11**) caused the molecule's activity against AChE to decrease. When we look at bis-α-aminophosphonate derivatives, the methyl groups added to the structure increased the molecule's activity against AChE. Therefore, the IC50 value of 13 (43.32 μM) is higher than other bis-α-aminophosphonates. When 14, 15, and 16 are compared, each methyl group added to the structure caused the molecule to show stronger inhibition against AChE. According to the results shown in Table 2, the synthesized bis-α-aminophosphonate derivatives demonstrated lower inhibition activity against AChE than their precursors Schiff bases derivatives. Table 2 also showed that new synthesized **14, 15** and **16** compounds were more potent than pyridostigmine bromide against acetylcholinesterase. The IC_{50} values of the synthesized **7–11** compounds against BChE are between 315.07 and 693.15 μM, while these values for **13–16** vary from 49.51 to 231.05 μM (Table 2). Looking at the results in Table 2, the synthesized Schiff bases exhibited low inhibition activity against BChE. However, **13** showed better inhibitor activities with IC_{50}=49.51 μM, compared to the pyridostigmine bromide (IC_{50}= 141.50 μM). Compared to the previous observations, our tested bis-a-aminophosphonate derivatives (**14–16**) exhibited stronger inhibitory activity than bis-α-aminophosphonates containing diphenyl moieties (IC_{50}=34.13–85.04 μg/mL) [62].

3.4. *Enzyme kinetics*

Based on kinetic inhibition study on the AChE enzyme, the most effective bis-α-aminophosphonate derivatives—compounds **14, 15**, and

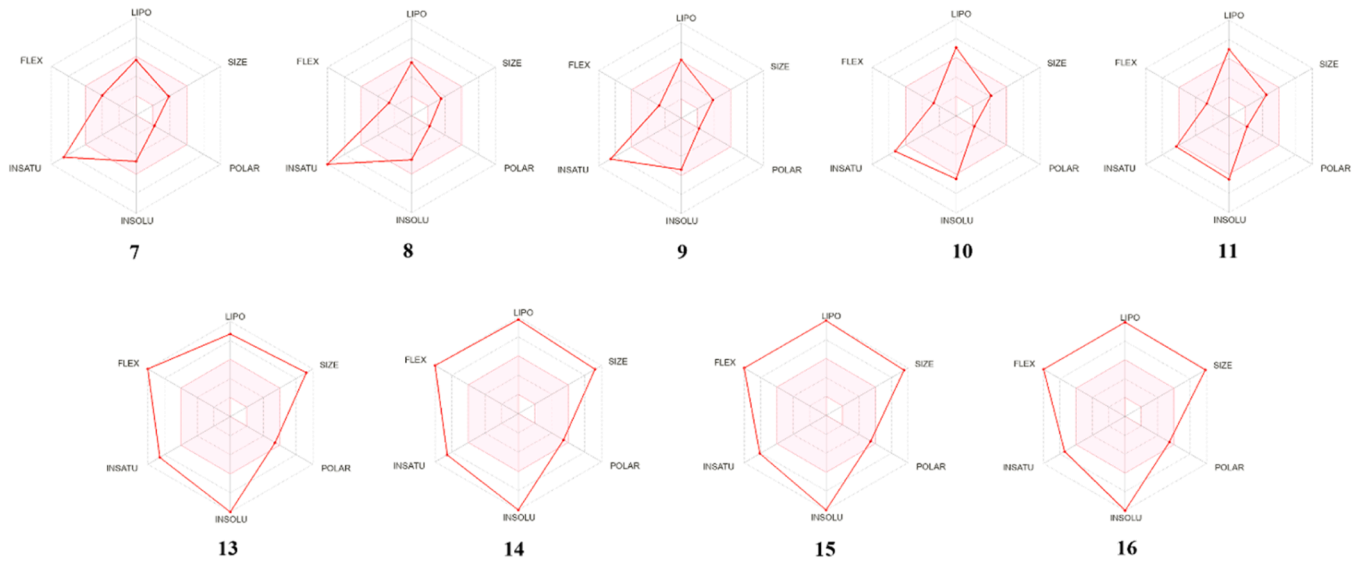

Fig. 15. Bioavailability radars of Schiff bases **7**–**11** and bis-α-aminophosphonates **13**–**16**.

16— were further examined to provide insight into a potential mechanism of inhibition. Here, AChE was tested using fixed doses of inhibitors **14, 15**, and **16** with different concentrations of the ATChI substrate. Using Lineweaver Burk plots, the [K_m], [V_{max}], and mode of inhibition data for **14, 15**, and **16** were computed and visualized in Fig. 3. According to the results from Lineweaver–Burk plots, it was determined that **14, 15**, and **16** non-competitively bind to a binding site of the enzyme, which is differ from the active site. K_i values for compounds **14, 15,** and **16** were calculated as 25.26 ± 8.32, 19.61 ± 10.81, and 22.54 ± 7.15, respectively.

3.5. Molecular docking

As a result of enzyme kinetic studies, it was observed that the synthesized compounds were non-competitive inhibitors against AChE. In this type of inhibition, the inhibitor binds to a place outside the active site of the enzyme. Regions to which compounds could bind, other than the active region, were determined using the Molegro Virtual Docker program. Then, the binding scores of the ligands in each active site determined were individually calculated. The determined binding sites with box coordinates for AChE and MolDock scores of ligands are shown in Fig. 4. As seen in Fig. 4, it was determined that binding site 1 (X, Y, Z coordinates: −3.25, −36.25, 11.00) possesses the best binding score. The calculated MolDock scores and hydrogen bonding of the compounds are presented in Table 3.

Fig. 5 shows the 2D and 3D diagram of the complex formed by AChE and compound **14** and the surface (gray) of the protein interacting with compound **14** (yellow) at the binding site. Compound **14** was bound to Pro235 in the respective binding site of AChE via conventional hydrogen bonding (Fig. 3). Compound **14** interacted with Glu313, located in the same site of the corresponding enzyme, through electrostatic interaction, that is, π-anion. It has been observed that there is a hydrophobic type of interaction (alkyl and π-alkyl) between Pro537, Val303, Arg296, Pro290, Leu289, Pro368, Val370 and Pro410 and compound **14**.

Fig. 6 shows the 2D and 3D diagram of the complex formed by AChE and compound **15** and the surface (gray) of the protein interacting with compound **15** (blue) at the binding site.

It has been observed that the benzene ring bound of nitrogen in compound **15** interacts with Arg296 in the binding site of the enzyme and forms a π-cation bond. In addition, in such site of the AChE, alkyl and π-alkyl interaction are formed between Pro410, Cys409, Trp532, Pro537, Leu540, Val303, Pro290, and Leu289 and compound **15** (via hydrophobic interaction).

Fig. 7 shows the 2D and 3D diagram of the complex formed by AChE and compound **16** and the surface (gray) of the protein interacting with compound **16** (pink) at the binding site. Compound **16** is attached to Pro235 and Arg296 in the corresponding binding site of AChE by hydrogen bonding (Fig. 5). The nitrogen-bound benzene ring in compound **16** interacts with His405 via π-π interaction, whereas the phosphorus-bound phenoxy group interacts with Glu313 at the enzyme's binding site via π-anion interaction. It has been observed that there is a hydrophobic type of interaction (alkyl and π-alkyl) between, Val239, Pro290, Pro368, Val370, Cys409, Pro410, Trp532, Leu536, Pro537, and Leu540 and compound **16**.

3.6. Molecular dynamic simulations of AChE protein, as apoprotein and in complex with compounds 14 and 15

In order to evaluate the binding interactions between the AChE protein (PDB ID: 4EY7) and two specific compounds, compounds **14** and **15**, a series of molecular dynamics (MD) simulations were conducted. These simulations, each lasting 100 nanoseconds, encompassed three distinct models: the Apoprotein AChE, the compound **14**-AChE complex, and the compound **15**-AChE complex, as illustrated in Fig. 8. Through these simulations, a comprehensive analysis was performed, encompassing various statistical parameters such as Root-Mean-Square Deviation (RMSD), Root-Mean-Square Fluctuation (RMSF), as well as the characterization of hydrogen bond interactions and their respective occupancy percentages over the duration of the simulations.

3.6.1. RMSD analysis

Finding out how the protein and ligand's structures changed throughout the course of the simulation is a lot easier when you look at the Root-Mean-Square Deviation (RMSD). The RMSD of the protein over time for two different simulations is shown in Fig. 9 in a multiplot. With RMSD values dropping below 0.5 nm, it is clear that all compounds achieved a stable phase.

The Root-Mean-Square Deviation (RMSD) values of the ligands offer valuable insights into the stability of their interactions with the protein. Fig. 10, we can see the ligands' RMSD throughout all simulations shown on a multiplot graph. The RMSD values of both ligands are consistently less than 0.2 nm, which is rather interesting. The RMSD readings of compound **15** are more consistently steady than those of compound **14**, however. Nevertheless, collectively, both ligands have demonstrated RMSD values within acceptable limits, indicating their effective ability to bind with the AChE protein.

Table 5
Drug likeness features of synthesized Schiff bases using Swiss ADME.

Compound		7	8	9	10	11
Physicochemical Properties	Molecular weight (g/mol)	312.41	284.35	312.41	340.46	368.51
	Num. heavy atoms	24	22	24	26	28
	Num. arom. heavy atoms	18	18	18	18	18
	Fraction Csp3	0.09	0.00	0.09	0.17	0.23
	Num. rotatable bonds	6	4	4	4	4
	Num. H-bond acceptors	2	2	2	2	2
	Num. H-bond donors	0	0	0	0	0
	Molar Refractivity	102.33	93.83	103.77	113.70	123.63
	TPSA (Å^2)	24.72	24.72	24.72	24.72	24.72
Lipophilicity	Log $P_{o/w}$ (iLOGP)	3.63	3.34	3.88	4.22	4.68
	Log $P_{o/w}$ (XLOGP3)	4.39	4.12	5.25	6.81	6.71
	Log $P_{o/w}$ (WLOGP)	4.62	5.19	5.80	6.42	7.04
	Log $P_{o/w}$ (MLOGP)	3.92	4.02	4.46	4.88	5.30
	Log $P_{o/w}$ (SILICOS-IT)	6.60	5.83	6.86	7.90	8.96
	Consensus Log $P_{o/w}$	4.63	4.50	5.25	6.05	6.54
Water Solubility	Log *S* (ESOL)	−4.70	−4.54	−5.38	−6.49	−6.56
	Solubility	6.21e-03 mg/ml; 1.99e-05 mol/l	8.20e-03 mg/ml; 2.88e-05 mol/l	1.32e-03 mg/ml; 4.21e-06 mol/l	1.10e-04 mg/ml; 3.24e-07 mol/l	1.01e-04 mg/ml; 2.73e-07 mol/l
	Class	Moderately soluble	Moderately soluble	Moderately soluble	Poorly soluble	Poorly soluble
Pharmacokinetics	GI absorption	High	High	High	High	Low
	BBB permeant	Yes	Yes	Yes	No	No
	P-gp substrate	No	No	Yes	Yes	Yes
	CYP1A2 inhibitor	Yes	Yes	Yes	No	No
	CYP2C19 inhibitor	Yes	Yes	Yes	Yes	No
	CYP2C9 inhibitor	No	Yes	No	No	No
	CYP2D6 inhibitor	No	No	No	No	No
	CYP3A4 inhibitor	Yes	Yes	Yes	Yes	Yes
	Log K_p (skin permeation)	−5.09 cm/s	−5.11 cm/s	−4.48 cm/s	−3.54 cm/s	−3.78 cm/s
Druglikeness	Lipinski	Yes; 0 violation	Yes; 0 violation	Yes; 1 violation: MLOGP>4.15	Yes; 1 violation: MLOGP>4.15	Yes; 1 violation: MLOGP>4.15
	Ghose	Yes	Yes	No; 1 violation: WLOGP>5.6	No; 1 violation: WLOGP>5.6	No; 1 violation: WLOGP>5.6
	Veber	Yes	Yes	Yes	Yes	Yes
	Egan	Yes	Yes	Yes	No; 1 violation: WLOGP>5.88	No; 1 violation: WLOGP>5.88
	Muegge	Yes	Yes	No; 1 violation: XLOGP3>5	No; 1 violation: XLOGP3>5	No; 1 violation: XLOGP3>5
	Bioavailability Score	0.55	0.55	0.55	0.55	0.55
Medicinal Chemistry	PAINS	0 alert	0 alert	0 alert	0 alert	0 alert
	Brenk	1 alert: imine_1	1 alert: imine_1	1 alert: imine_1	1 alert: imine_1	1 alert: imine_1
	Leadlikeness	No; 1 violation: XLOGP3>3.5	No; 1 violation: XLOGP3>3.5	No; 1 violation: XLOGP3>3.5	No; 1 violation: XLOGP3>3.5	No; 2 violations: MW>350, XLOGP3>3.5
	Synthetic accessibility	2.88	2.46	2.71	3.00	3.23

3.6.2. *RMSF analysis*

Examining the Root-Mean-Square Fluctuation (RMSF) of the protein provides valuable insights into localized structural changes. Fig. 11 presents a multiplot graph illustrating the protein's RMSF, measured in nanometers, corresponding to the residue number index. It's crucial to note that this graph indicates fluctuations of less than 0.6 nm for the majority of protein residues, affirming the overall structural stability. However, higher fluctuations were observed, particularly in the enzyme region Ser309-Gln369, in the case of compound **14**. Conversely, relatively elevated fluctuations were noted for compound **15** at residues Ser215, Gly220, His432, and Glu450 throughout the 100 nanoseconds simulation period.

3.6.3. *H-Bond interaction*

Understanding molecular interactions, particularly hydrogen bonds (H-bonds), relies on both distance and angle parameters and can be affected by dynamic conditions. In this investigation, we analyzed H-bond interactions within the complexes. Fig. 12 is a graph that shows the amount of hydrogen bonding as a function of time. Compound **15** showed stronger and more constant H-bond interactions than compound **14** throughout the simulation, as shown in the figure. We computed the percentage occupancies of certain residues involved in these H-bond interactions to investigate these interactions further and assess their stability.

Fig. 13 illustrates a histogram presenting the percentage occupancies of hydrogen bond contacts formed by different ligands. This graph highlights compound **14**′s ability to establish multiple interactions with Gln250, His287, and Tyr341 of the AChE protein, with occupancy rates of 11.16 %, 5.24 %, and 3.96 %, respectively. Conversely, compound **15** demonstrates stable hydrogen bond interactions with residues Tyr72, Trp286, Ser293, Phe295, and Arg296, which persisted for 8.84 %, 23.31 %, 38.26 %, 43.06 %, and 6.90 % of the simulation period, respectively. Upon comparing occupancy rates with AChE residues, it becomes evident that compound **15** forms a more effective and stable complex structure with the protein. In summary, these findings suggest that among the two ligands, compound **15** appears to be the most efficient in

Table 6
Drug likeness features of synthesized bis-α-aminophosphonates using Swiss ADME.

Compound		13	14	15	16
Physicochemical Properties	Molecular weight (g/mol)	780.78	780.78	808.84	836.89
	Num. heavy atoms	56	56	58	60
	Num. arom. heavy atoms	42	42	42	42
	Fraction Csp3	0.09	0.09	0.12	0.16
	Num. rotatable bonds	18	16	16	16
	Num. H-bond acceptors	8	6	6	6
	Num. H-bond donors	2	2	2	2
	Molar Refractivity	221.94	225.34	235.27	245.20
	TPSA (Å^2)	114.74	114.74	114.74	114.74
Lipophilicity	Log $P_{o/w}$ (iLOGP)	5.20	5.48	6.09	6.31
	Log $P_{o/w}$ (XLOGP3)	9.66	11.62	12.35	13.08
	Log $P_{o/w}$ (WLOGP)	11.01	12.20	12.81	13.43
	Log $P_{o/w}$ (MLOGP)	6.10	6.64	6.96	7.27
	Log $P_{o/w}$ (SILICOS-IT)	6.98	7.24	8.34	9.44
	Consensus Log $P_{o/w}$	7.79	8.63	9.31	9.91
Water Solubility	Log *S* (ESOL)	−10.13	−11.50	−12.12	−12.73
	Solubility	5.74e-08 mg/ml; 7.35e-11 mol/l	2.47e-09 mg/ml; 3.16e-12 mol/l	6.20e-10 mg/ml; 7.67e-13 mol/l	1.55e-10 mg/ml; 1.86e-13 mol/l
	Class	Insoluble	Insoluble	Insoluble	Insoluble
Pharmacokinetics	GI absorption	Low	Low	Low	Low
	BBB permeant	No	No	No	No
	P-gp substrate	No	Yes	Yes	Yes
	CYP1A2 inhibitor	No	No	No	No
	CYP2C19 inhibitor	No	No	No	No
	CYP2C9 inhibitor	No	No	No	No
	CYP2D6 inhibitor	No	No	No	No
	CYP3A4 inhibitor	No	No	No	No
	Log K_p (skin permeation)	−4.20 cm/s	−2.81 cm/s	−2.47 cm/s	−2.12 cm/s
Druglikeness	Lipinski	No; 2 violations: MW>500, MLOGP>4.15	No; 2 violations: MW>500, MLOGP>4.15	No; 2 violations: MW>500, MLOGP>4.15	No; 2 violations: MW>500, MLOGP>4.15
	Ghose	No; 4 violations: MW>480, WLOGP>5.6, MR>130, #atoms>70	No; 4 violations: MW>480, WLOGP>5.6, MR>130, #atoms>70	No; 4 violations: MW>480, WLOGP>5.6, MR>130, #atoms>70	No; 4 violations: MW>480, WLOGP>5.6, MR>130, #atoms>70
	Veber	No; 1 violation: Rotors>10	No; 1 violation: Rotors>10	No; 1 violation: Rotors>10	No; 1 violation: Rotors>10
	Egan	No; 1 violation: WLOGP>5.88	No; 1 violation: WLOGP>5.88	No; 1 violation: WLOGP>5.88	No; 1 violation: WLOGP>5.88
	Muegge	No; 3 violations: MW>600, XLOGP3>5, Rotors>15	No; 3 violations: MW>600, XLOGP3>5, Rotors>15	No; 3 violations: MW>600, XLOGP3>5, Rotors>15	No; 3 violations: MW>600, XLOGP3>5, Rotors>15
	Bioavailability Score	0.17	0.17	0.17	0.17
Medicinal Chemistry	PAINS	0 alert	0 alert	0 alert	0 alert
	Brenk	1 alert: phosphor	1 alert: phosphor	1 alert: phosphor	1 alert: phosphor
	Leadlikeness	No; 3 violations: MW>350, Rotors>7, XLOGP3>3.5	No; 3 violations: MW>350, Rotors>7, XLOGP3>3.5	No; 3 violations: MW>350, Rotors>7, XLOGP3>3.5	No; 3 violations: MW>350, Rotors>7, XLOGP3>3.5
	Synthetic accessibility	6.61	6.52	6.80	7.06

binding with the AChE protein.

3.6.4. MMGBSA calculations

As part of the molecular dynamics investigation, a thorough energetics analysis was performed, which included MMGBSA calculations Fig. 14. This analysis revealed average ΔG values of −64.22 kcal/mol for compound **14** and −86.11 kcal/mol for compound **15** (Table 4). These results indicate the superior efficiency of compound **15** in binding with the AChE protein. With such findings, compound **15** emerges as a highly promising candidate for future pharmacological studies, particularly for its potential as an agent of Alzheimer's disease.

3.7. In silico ADME and toxicity analysis

Fig. 15 shows the bioavailability radars of all synthesized compounds (**7**–**11** and **13**–**16**). The pink field in Fig. 15 stands for the optimal range for each feature (Lipo: Lipophilicity, Size: Moleculer weight, Polar: Total Polar Surface Area, Insolu: Insolubility, Insatu: Insaturation, Flex: Flexibility). In this study, we also examined the physicochemical, lipophilicity, solubility, pharmacokinetics, drug similarity, and medicinal chemistry properties of the synthesized compounds. In drug discovery and development, a molecule must have both high bioactivity and low toxicity [63]. The organism's ability to reach and concentrate on the therapeutic target is equally crucial [63]. Early ADME (Absorption, Distribution, Metabolism, and Excretion) estimation during the discovery phase has been shown to significantly lower the percentage of pharmacokinetics-related failure during the clinical phases [63]. The molecule's permeability through the skin decreases with increasing negative skin permeability (Log K_p). The Log K_p value of all compounds is between –2.12 and –5.11 cm/s. For instance, compound **7** has low skin

permeability (Log K_p = –5.11 cm/s), while compound **16** has good skin permeability (Log K_p = –2.12 cm/s). The topological polar surface area (TPSA) for polarity should be in the range of 20 to 130 Å^2. TPSA of all studied compounds is between 20 and 130 Å^2. The compounds' synthetic accessibility scores range from 1 (very easy) to 10 (extremely difficult). Considering the results of ADME given in Tables 5 and 6, it appears that the synthetic accessibility of Schiff base compounds is better than that of bis-α-aminophosphonate compounds. Approximately –10 (insoluble), –6 (poorly soluble), –4 (soluble), –2 (extremely soluble), and 0 (very soluble) are the values on the solubility (log S) scale. The solubility of **13** - **16** is detected as insoluble. The **7** - **9** are found to be moderately soluble and **10** and **11** are poorly soluble. While compounds **7, 8,** and **9** pass the Blood-Brain Barrier, other compounds cannot pass through the Blood-Brain Barrier. According to Lipinski's rule of five, a molecule that can be a drug must have molecular weight (MW) $\leq$ 500 g/mol, lipophilicity (log P) $\leq$ 5, hydrogen-bond donor $\leq$ 5, hydrogen-bond acceptor $\leq$ 10 and molar refractivity (MR) value between 4 and 130. According to Lipinski's above-mentioned parameters and other physicochemical properties from the ADME study, which all is presented in Table 5, compounds **7** and **8** could be a potential drug agent.

4. Conclusion

In the present study, novel Schiff bases (**7**–**11**) and bis-α-aminophosphonate derivatives (**13**–**16**) are designed and synthesized to investigate the inhibitory properties against AChE and BChE enzymes by determining their IC_{50} and K_i values. Kinetic studies showed that the inhibition mechanism of **14** - **16** against AChE is non-competitive. Among bis-α-aminophosphonates, **14** - **16** demonstrated strong inhibition against AChE (IC_{50}= 6.48, 9.00, and 10.88 μM, respectively) in comparison to positive control pyridostigmine bromide (IC_{50}= 26.2 μM). Compared to the synthesized Schiff bases, bis-α-aminophosphonates showed better inhibition, which is thought to be due to the phosphonate groups attached to the Schiff bases. Furthermore, molecular docking studies were also performed, and as a result, non-covalent interactions between compounds and AChE were presented. To assess how well compounds **14** and **15** bind to the AChE, we performed an extra round of molecular dynamics simulations. MD findings suggest that compounds **14** and **15** display significant affinity towards the AChE protein. In addition, MMGBSA calculations demonstrated the average ΔG values of −64.22 kcal/mol for compound **14** and −86.11 kcal/mol for compound **15**. The agreement between experimental inhibition, molecular docking, and molecular dynamic findings has mutually validated them. This significant finding suggests that compound **15** may have potential in Alzheimer's disease treatment by modulating AChE protein activity.

CRediT authorship contribution statement

Emel Ekinci: Writing – review & editing, Writing – original draft, Visualization, Validation, Resources, Methodology, Investigation, Formal analysis, Data curation, Conceptualization. **Harun Çiftçi:** Writing – review & editing, Validation, Supervision, Resources, Methodology, Investigation, Funding acquisition, Formal analysis, Conceptualization. **Şevki Adem:** Writing – review & editing, Validation, Supervision, Resources, Methodology, Investigation, Funding acquisition, Formal analysis, Data curation, Conceptualization. **Özlem Gündoğdu Aytaç:** Writing – review & editing, Writing – original draft, Visualization, Resources, Methodology, Investigation, Funding acquisition, Data curation. **Volkan Eyüpoğlu:** Writing – review & editing, Writing – original draft, Visualization, Software, Methodology, Investigation, Formal analysis, Data curation, Conceptualization.

Declaration of competing interest

The authors declare that they have no known competing financial interests or personal relationships that could have appeared to influence the work reported in this paper.

Acknowledgments

This work was financially supported by The Scientific Research Projects Coordination Office of Çankırı Karatekin University (BAP, Project No: FF081123D05). The computations reported in this study were partially performed at TUBITAK ULAKBIM High Performance and Grid Computing Center (TRUBA resources).

Supplementary materials

Supplementary material associated with this article can be found, in the online version, at doi:10.1016/j.molstruc.2025.141734.

Data availability

Data will be made available on request.

References

[1] A. Alam, G. Ali, A. Nawaz, T.S. AlOmar, A. Rauf, M. Ayaz, S. Ahmad, N. Almasoud, A.S. AlOmar, A.A. Khalil, P. Wilairatana, Neuroprotective evaluation of diospyrin against drug-induced Alzheimer's disease, Fitoterapia 171 (2023) 105703, https://doi.org/10.1016/j.fitote.2023.105703.
[2] D. Wan, F.-Q. Wang, J. Xie, L. Chen, X.-L. Zhou, Design, synthesis, and biological activity of Donepezil: aromatic amine hybrids as anti-alzheimerss drugs, ACS. Omega 8 (2023) 21802–21812, https://doi.org/10.1021/acsomega.3c01427.
[3] M. Taha, F. Rahim, A.A. Khan, B. Adalat, S. Imran, J.M. Alshehri, A. Ahmad, K. M. Khan, S.A.A. Shah, N. Uddin, The β-carboline analogs as a potent inhibitor for Alzheimer's Disease, molecular docking and dynamics simulation study, Arab. J. Chem. 16 (2023) 105300, https://doi.org/10.1016/j.arabjc.2023.105300.
[4] J. Lisa-Molina, P. Gómez-Murillo, I. Arellano-Martín, C. Jiménez, M.L. Rodríguez-Escobar, L.R. Tallini, F. Viladomat, L. Torras-Claveria, J. Bastida, Alkaloid profile in wild autumn-flowering daffodils and their acetylcholinesterase inhibitory activity, Molecules. 28 (2023) 1239, https://doi.org/10.3390/molecules28031239.
[5] Dementia, (n.d.). https://www.who.int/news-room/fact-sheets/detail/dementia (accessed December 11, 2023).
[6] H. Hampel, M.-M. Mesulam, A.C. Cuello, M.R. Farlow, E. Giacobini, G. T. Grossberg, A.S. Khachaturian, A. Vergallo, E. Cavedo, P.J. Snyder, Z. S. Khachaturian, The cholinergic system in the pathophysiology and treatment of Alzheimer's disease, Brain 141 (2018) 1917–1933, https://doi.org/10.1093/brain/awy132.
[7] A. Nazarian, F. Abedinifar, H. Hamedifar, M.H. Hashempur, M. Mahdavi, N. Sepehri, A. Iraji, Anticholinesterase activities of novel isoindolin-1,3-dione-based acetohydrazide derivatives: design, synthesis, biological evaluation, molecular dynamic study, BMC. Chem. 18 (2024) 64, https://doi.org/10.1186/s13065-024-01169-4.
[8] N. Oliyaei, M. Moosavi-Nasab, N. Tanideh, A. Iraji, Multiple roles of fucoxanthin and astaxanthin against Alzheimer's disease: their pharmacological potential and therapeutic insights, Brain Res. Bull. 193 (2023) 11–21, https://doi.org/10.1016/j.brainresbull.2022.11.018.
[9] M. Saeedi, A. Maleki, A. Iraji, R. Hariri, T. Akbarzadeh, N. Edraki, O. Firuzi, S. S. Mirfazli, Synthesis and bio-evaluation of new multifunctional methylindolinone-1,2,3-triazole hybrids as anti-Alzheimer's agents, J. Mol. Struct. 1229 (2021) 129828, https://doi.org/10.1016/j.molstruc.2020.129828.
[10] K. Sharma, Cholinesterase inhibitors as Alzheimer's therapeutics (Review), Mol. Med. Rep. 20 (2019) 1479–1487, https://doi.org/10.3892/mmr.2019.10374.
[11] S. Jaipea, N. Saehlim, W. Sutcharitruk, A. Athipornchai, K. Ingkaninan, R. Saeeng, Synthesis of piperine analogues as AChE and BChE inhibitors for the treatment of Alzheimer's disease, Phytochem. Lett. 53 (2023) 216–221, https://doi.org/10.1016/j.phytol.2023.01.004.
[12] M. Eddahmi, G. La Spada, A. Hafid, M. Khouili, M. Catto, L. Bouissane, Towards Alzheimer's disease-related targets: one-pot Cu(I)- mediated synthesis of new nitroindazolyltriazoles, Bioorg. Chem. 130 (2023) 106261, https://doi.org/10.1016/j.bioorg.2022.106261.
[13] R.J. Obaid, N. Naeem, E.U. Mughal, M.M. Al-Rooqi, A. Sadiq, R.S. Jassas, Z. Moussa, S.A. Ahmed, Inhibitory potential of nitrogen, oxygen and sulfur containing heterocyclic scaffolds against acetylcholinesterase and butyrylcholinesterase, RSC. Adv. 12 (2022) 19764–19855, https://doi.org/10.1039/D2RA03081K.

[14] N. Žnidaršič, M. Štrbenc, N. Grgurevič, T. Snoj, Potential revival of cholinesterase inhibitors as drugs in veterinary medicine, Front. Vet. Sci. 10 (2023), https://doi.org/10.3389/fvets.2023.1125618.
[15] M. Saeedi, A. Maleki, A. Iraji, R. Hariri, T. Akbarzadeh, N. Edraki, O. Firuzi, S. S. Mirfazli, Synthesis and bio-evaluation of new multifunctional methylindolinone-1,2,3-triazole hybrids as anti-Alzheimer's agents, J. Mol. Struct. 1229 (2021) 129828, https://doi.org/10.1016/j.molstruc.2020.129828.
[16] M. Gopalakrishnan, P. Sureshkumar, V. Kanagarajan, J. Thanusu, New environmentally-friendly solvent-free synthesis of imines using calcium oxide under microwave irradiation, Res. Chem. Intermed. 33 (2007) 541–548, https://doi.org/10.1163/156856707782565822.
[17] S. Das, V.K. Das, L. Saikia, A.J. Thakur, Environment-friendly and solvent-free synthesis of symmetrical bis-imines under microwave irradiation, Green. Chem. Lett. Rev. 5 (2012) 457–474, https://doi.org/10.1080/17518253.2012.667443.
[18] S. Aytac, O. Gundogdu, Z. Bingol, İ. Gulcin, Synthesis of schiff bases containing phenol rings and investigation of their antioxidant capacity, anticholinesterase, butyrylcholinesterase, and carbonic anhydrase inhibition properties, Pharmaceutics. 15 (2023) 779, https://doi.org/10.3390/pharmaceutics15030779.
[19] Politeknik Dergisi » Makale » Yeni Schiff Bazı Bileşiklerinin Sentezi ve Yapılarının Aydınlatılması, (n.d.). https://dergipark.org.tr/tr/pub/politeknik/article/382621 (accessed January 20, 2025).
[20] B. Ermiş, E. Ekinci, U. Bozkaya, State-of-the-art computations of vertical electron affinities with the extended Koopmans' Theorem integrated with the CCSD(T) method, J. Chem. Theory. Comput. 17 (2021) 7648–7656, https://doi.org/10.1021/acs.jctc.1c00938.
[21] S. Shokrollahi, A. Amiri, F. Fadaei-Tirani, K. Schenk-Joß, Promising anti-cancer potency of 4,5,6,7-tetrahydrobenzo[d]thiazole-based Schiff-bases, J. Mol. Liq. 300 (2020) 112262, https://doi.org/10.1016/j.molliq.2019.112262.
[22] R. Shukla, A.P. Singh, P.K. Sonar, M. Mishra, S.K. Saraf, Schiff bases of benzothiazol-2-ylamine and Thiazolo[5,4-b] pyridin-2-ylamine as anticonvulsants: synthesis, characterization and toxicity profiling, Cent. Nerv. Syst. Agents Med. Chem. 16 (2016) 240–248, https://doi.org/10.2174/1871524916666160428110728.
[23] M.S. More, P.G. Joshi, Y.K. Mishra, P.K. Khanna, Metal complexes driven from Schiff bases and semicarbazones for biomedical and allied applications: a review, Mater. Today Chem. 14 (2019) 100195, https://doi.org/10.1016/j.mtchem.2019.100195.
[24] T. Tunç, Z. Alım, Synthesis of new schiff bases and assessment of their in vitro biological effects on acetylcholinesterase and carbonic anhydrase isoenzymes activities, Russ. J. Org. Chem. 57 (2021) 247–254, https://doi.org/10.1134/S1070428021020160.
[25] M. Gundluru, S. Sarva, M.K.R. Kandula, V.R. Netala, V. Tartte, S.R. Cirandur, Phosphosulfonic acid-catalyzed green synthesis and bioassay of α-aryl-α′-1,3,4-thiadiazolyl aminophosphonates, Heteroatom Chem. 27 (2016) 269–278, https://doi.org/10.1002/hc.21325.
[26] A. Amira, Z. Aouf, H. K'tir, Y. Chemam, R. Ghodbane, R. Zerrouki, N.-E. Aouf, Recent advances in the synthesis of α-aminophosphonates: a review, ChemistrySelect. 6 (2021) 6137–6149, https://doi.org/10.1002/slct.202101360.
[27] M.H. Baren, S.A. Ibrahim, M.M. Al-Rooqi, S.A. Ahmed, M.M. El-Gamil, H.A. Hekal, A new class of anticancer activity with computational studies for a novel bioactive aminophosphonates based on pyrazole moiety, Sci. Rep. 13 (2023) 14680, https://doi.org/10.1038/s41598-023-40265-8.
[28] H.S.A. Mandour, M.A. Hamed, K.M. Saad-Allah, M.K. Abd Elnabi, H.A. Abosharaf, A.A. El-Gharably, Antimicrobial and molecular docking studies of novel synthesized α-aminophosphonates based on pyrozol moiety as anticancer agents via α-topoisomerase II inhibition, ChemistrySelect. 8 (2023) e202300254, https://doi.org/10.1002/slct.202300254.
[29] S. Shaikh, P. Dhavan, G. Pavale, M.M.V. Ramana, B.L. Jadhav, Design, synthesis and evaluation of pyrazole bearing α-aminophosphonate derivatives as potential acetylcholinesterase inhibitors against Alzheimer's disease, Bioorg. Chem. 96 (2020) 103589, https://doi.org/10.1016/j.bioorg.2020.103589.
[30] J.J. Uparkar, P.P. Dhavan, B.L. Jadhav, S.D. Pawar, Design, synthesis and biological evaluation of furan based α-aminophosphonate derivatives as anti-alzheimer agent, J. Iran Chem. Soc. 19 (2022) 3103–3116, https://doi.org/10.1007/s13738-022-02515-w.
[31] K.Y. Rao, S.J. Basha, K. Monika, M. Sreelakshmi, I. Sivakumar, G. Mallikarjuna, R. M. Yadav, S. Kumar, R. Subramanyam, A.G. Damu, Synthesis and anti-alzheimer potential of novel α-amino phosphonate derivatives and probing their molecular interaction mechanism with acetylcholinesterase, Eur. J. Med. Chem. 253 (2023) 115288, https://doi.org/10.1016/j.ejmech.2023.115288.
[32] B. Kaboudin, S. Faghih, S. Alavi, M.R. Naimi-Jamal, A. Fattahi, An efficient one-pot synthesis of 1-aminophosphonates, Synthesis (Mass) 55 (2023) 121–130, https://doi.org/10.1055/a-1941-1242.
[33] A.D. Becke, Density-functional thermochemistry. III. The role of exact exchange, J. Chem. Phys. 98 (1993) 5648–5652. https://doi.org/10.1063/1.464913.</bib.
[34] C. Lee, W. Yang, R.G. Parr, Development of the Colle-Salvetti correlation-energy formula into a functional of the electron density, Phys. Rev. B 37 (1988) 785–789, https://doi.org/10.1103/PhysRevB.37.785.
[35] T.H. Dunning Jr., Gaussian basis sets for use in correlated molecular calculations. I. The atoms boron through neon and hydrogen, J. Chem. Phys. 90 (1989) 1007–1023, https://doi.org/10.1063/1.456153.
[36] S. Manap, H. Medetalibeyoğlu, A. Kılıç, O.F. Karataş, B. Tüzün, M. Alkan, A. B. Ortaakarsu, A. Atalay, M. Beytur, H. Yüksek, Synthesis, molecular modeling investigation, molecular dynamic and ADME prediction of some novel Mannich bases derived from 1,2,4-triazole, and assessment of their anticancer activity, J. Biomol. Struct. Dyn. 0 (2023) 1–15, https://doi.org/10.1080/07391102.2023.2265501.
[37] O. Akyıldırım, H. Medetalibeyoğlu, E. Oğuz, A. Aras, A. Atalay, A. Korkmaz, M. Beytur, F. Türkan, H. Yüksek, Novel Mannich bases derived from 1,2,4-triazoles: design, synthesis, characterization, and glutathione S-transferase inhibition properties investigations, J. Mol Struct 1293 (2023) 136321, https://doi.org/10.1016/j.molstruc.2023.136321.
[38] M.J. Frisch, G.W. Trucks, H.B. Schlegel, G.E. Scuseria, M.A. Robb, J.R. Cheeseman, G. Scalmani, V. Barone, B. Mennucci, G.A. Petersson, H. Nakatsuji, M. Caricato, X. Li, H.P. Hratchian, A.F. Izmaylov, J. Bloino, G. Zheng, J.L. Sonnenberg, M. Hada, M. Ehara, K. Toyota, R. Fukuda, J. Hasegawa, M. Ishida, T. Nakajima, Y. Honda, O. Kitao, H. Nakai, T. Vreven, J.A. Montgomery Jr., J.E. Peralta, F. Ogliaro, M. Bearpark, J.J. Heyd, E. Brothers, K.N. Kudin, V.N. Staroverov, R. Kobayashi, J. Normand, K. Raghavachari, A. Rendell, J.C. Burant, S.S. Iyengar, J. Tomasi, M. Cossi, N. Rega, J.M. Millam, M. Klene, J.E. Knox, J.B. Cross, V. Bakken, C. Adamo, J. Jaramillo, R. Gomperts, R.E. Stratmann, O. Yazyev, A.J. Austin, R. Cammi, C. Pomelli, J.W. Ochterski, R.L. Martin, K. Morokuma, V.G. Zakrzewski, G.A. Voth, P. Salvador, J.J. Dannenberg, S. Dapprich, A.D. Daniels, O. Farkas, J.B. Foresman, J. V. Ortiz, J. Cioslowski, and D.J. Fox, Gaussian 09, Revision B.01. Gaussian Inc., (2010). Wallingford.
[39] G.L. Ellman, K.D. Courtney, V. Andres, R.M. Featherstone, A new and rapid colorimetric determination of acetylcholinesterase activity, Biochem. Pharmacol. 7 (1961) 88–95, https://doi.org/10.1016/0006-2952(61)90145-9.
[40] E. Coteli, B. Erdem, H. Ciftci, Phytochemical content of Malus floribunda, Vitro and Molecular Docking Studies, Appl Biochem Biotechnol (2023), https://doi.org/10.1007/s12010-023-04826-x.
[41] R. Thomsen, M.H. Christensen, MolDock: A new technique for high-accuracy molecular docking, J. Med. Chem. 49 (2006) 3315–3321, https://doi.org/10.1021/jm051197e.
[42] J. Cheung, M.J. Rudolph, F. Burshteyn, M.S. Cassidy, E.N. Gary, J. Love, M. C. Franklin, J.J. Height, Structures of Human acetylcholinesterase in complex with pharmacologically important ligands, J. Med. Chem. 55 (2012) 10282–10286, https://doi.org/10.1021/jm300871x.
[43] F. Nachon, E. Carletti, C. Ronco, M. Trovaslet, Y. Nicolet, L. Jean, P.-Y. Renard, Crystal structures of human cholinesterases in complex with huprine W and tacrine: elements of specificity for anti-Alzheimer's drugs targeting acetyl- and butyryl-cholinesterase, Biochem. J. 453 (2013) 393–399, https://doi.org/10.1042/BJ20130013.
[44] S. Wang, J. Xie, J. Pei, L. Lai, CavityPlus 2022 update: an integrated platform for comprehensive protein cavity detection and property analyses with user-friendly tools and cavity databases, J. Mol. Biol. 435 (2023) 168141, https://doi.org/10.1016/j.jmb.2023.168141.
[45] A. Ganesan, M.L. Coote, K. Barakat, Molecular dynamics-driven drug discovery: leaping forward with confidence, Drug Discov. Today 22 (2017) 249–269, https://doi.org/10.1016/j.drudis.2016.11.001.
[46] S.A. Arvindekar, S. Mohole, A. Patil, P. Mane, A. Arvindekar, S.N. Mali, B. Thorat, R. Rawat, S. Sharma, Molecular docking, QSAR, pharmacophore modeling, and dynamics studies of some chromone derivatives for the discovery of anti-breast cancer agents against hormone-dependent breast cancer, J. Biomol. Struct. Dyn. 41 (2023) 14757–14770, https://doi.org/10.1080/07391102.2023.2190803.
[47] N. Schmid, A.P. Eichenberger, A. Choutko, S. Riniker, M. Winger, A.E. Mark, W. F. van Gunsteren, Definition and testing of the GROMOS force-field versions 54A7 and 54B7, Eur. Biophys. J. 40 (2011) 843–856, https://doi.org/10.1007/s00249-011-0700-9.
[48] D.M. van Aalten, R. Bywater, J.B. Findlay, M. Hendlich, R.W. Hooft, G. Vriend, PRODRG, a program for generating molecular topologies and unique molecular descriptors from coordinates of small molecules, J. Comput. Aided. Mol. Des. 10 (1996) 255–262, https://doi.org/10.1007/BF00355047.
[49] P. Mark, L. Nilsson, Structure and dynamics of the TIP3P, SPC, and SPC/E water models at 298 K, J. Phys. Chem. A 105 (2001) 9954–9960, https://doi.org/10.1021/jp003020w.
[50] A leap-frog algorithm for stochastic dynamics: molecular simulation: Vol 1, No 3, (n.d.). https://www.tandfonline.com/doi/abs/10.1080/08927028808080941 (accessed April 3, 2024).
[51] H.J.C. Berendsen, D. van der Spoel, R. van Drunen, GROMACS: a message-passing parallel molecular dynamics implementation, Comput. Phys. Commun. 91 (1995) 43–56, https://doi.org/10.1016/0010-4655(95)00042-E.
[52] B. Hess, H. Bekker, H.J.C. Berendsen, J.G.E.M. Fraaije, LINCS: a linear constraint solver for molecular simulations, J Comput. Chem. 18 (1997) 1463–1472, https://doi.org/10.1002/(SICI)1096-987X(199709)18:12<1463::AID-JCC4>3.0.CO;2-H.
[53] M. Di Pierro, R. Elber, B. Leimkuhler, A stochastic algorithm for the isobaric-isothermal ensemble with ewald summations for all long range forces, J. Chem. Theory. Comput. 11 (2015) 5624–5637, https://doi.org/10.1021/acs.jctc.5b00648.
[54] W. Humphrey, A. Dalke, K. Schulten, VMD: visual molecular dynamics, J. Mol. Graph. 14 (1996) 33–38, https://doi.org/10.1016/0263-7855(96)00018-5.
[55] HeroMDAnalysis: an automagical tool for GROMACS-based molecular dynamics simulation analysis - PubMed, (n.d.). https://pubmed.ncbi.nlm.nih.gov/33496197/(accessed April 3, 2024).
[56] B. Sahu, R. Bhatia, D. Kaur, D. Choudhary, R. Rawat, S. Sharma, B. Kumar, Design, synthesis and biological evaluation of oxadiazole clubbed piperazine derivatives as potential antidepressant agents, Bioorg. Chem. 136 (2023) 106544, https://doi.org/10.1016/j.bioorg.2023.106544.
[57] Graphing with Gnuplot and Xmgr | Linux Journal, (n.d.). https://www.linuxjournal.com/article/1218 (accessed April 3, 2024).

[58] M. Ayaz, Ö. Gündoğdu, S. Aytaç, B. Erdem, H. Çiftçi, Y. Erdogdu, Microwave-assisted synthesis, characterizations, antimicrobial activities, and DFT studies on some pyridine derived Schiff bases, J. Mol. Struct. 1269 (2022) 133791, https://doi.org/10.1016/j.molstruc.2022.133791.

[59] H. K'tir, A. Amira, C. Benzaid, Z. Aouf, S. Benharoun, Y. Chemam, R. Zerrouki, N.-E. Aouf, Synthesis, bioinformatics and biological evaluation of novel α-aminophosphonates as antibacterial agents: DFT, molecular docking and ADME/T studies, J. Mol. Struct. 1250 (2022) 131635, https://doi.org/10.1016/j.molstruc.2021.131635.

[60] M. Khalid, M.A. Ullah, M. Adeel, M. Usman Khan, M.N. Tahir, A.A.C. Braga, Synthesis, crystal structure analysis, spectral IR, UV–Vis, NMR assessments, electronic and nonlinear optical properties of potent quinoline based derivatives: interplay of experimental and DFT study, J. Saudi Chem. Soc. 23 (2019) 546–560, https://doi.org/10.1016/j.jscs.2018.09.006.

[61] L. Qi, M.-C. Li, J.-C. Bai, Y.-H. Ren, H.-X. Ma, In vitro antifungal activities, molecular docking, and DFT studies of 4-amine-3-hydrazino-5-mercapto-1,2,4-triazole derivatives, Bioorg. Med. Chem. Lett. 40 (2021) 127902, https://doi.org/10.1016/j.bmcl.2021.127902.

[62] R. Aissa, S. Guezane-Lakoud, M. Toffano, L. Gali, L. Aribi-Zouioueche, Fiaud's Acid, a novel organocatalyst for diastereoselective bis α-aminophosphonates synthesis with in-vitro biological evaluation of antifungal, antioxidant and enzymes inhibition potential, Bioorg. Med. Chem. Lett. 41 (2021) 128000, https://doi.org/10.1016/j.bmcl.2021.128000.

[63] A. Daina, O. Michielin, V. Zoete, SwissADME: a free web tool to evaluate pharmacokinetics, drug-likeness and medicinal chemistry friendliness of small molecules, Sci. Rep. 7 (2017) 42717, https://doi.org/10.1038/srep42717.